Journal of Geophysical Research: Oceans

RESEARCH ARTICLE
10.1029/2017JC013514

Influence of River-Induced Fronts on Hydrocarbon Transport: A Multiplatform Observational Study

Yannis Androulidakis[1], Vassiliki Kourafalou[1], Tamay Özgökmen[1], Oscar Garcia-Pineda[2], Björn Lund[1], Matthieu Le Hénaff[3,4], Chuanmin Hu[5], Brian K. Haus[1], Guillaume Novelli[1], Cedric Guigand[1], HeeSook Kang[1], Lars Hole[6], and Jochen Horstmann[7]

[1]Department of Ocean Sciences, University of Miami/Rosenstiel School of Marine and Atmospheric Science, Miami, FL, USA, [2]WaterMapping LLC, Gulf Breeze, FL, USA, [3]University of Miami/Cooperative Institute for Marine and Atmospheric Studies, Miami, FL, USA, [4]NOAA/Atlantic Oceanographic and Meteorological Laboratory, Miami, FL, USA, [5]College of Marine Science, University of South Florida, St. Petersburg, FL, USA, [6]Division of Oceanography and Marine Meteorology, Norwegian Meteorological Institute, Bergen, Norway, [7]Helmholtz Zentrum Geesthacht, Geesthacht, Germany

Key Points:
- Investigation of hydrocarbon pathways over Northern Gulf of Mexico: observational study
- Influence of river-induced fronts on oil transport
- Identification of three potential hydrocarbon pathways under the influence of Mississippi River plume, wind conditions, and ocean dynamics

Correspondence to:
Y. Androulidakis,
iandroul@rsmas.miami.edu

Citation:
Androulidakis, Y., Kourafalou, V., Özgökmen, T., Garcia-Pineda, O., Lund, B., Le Hénaff, M., et al. (2018). Influence of river-induced fronts on hydrocarbon transport: A multiplatform observational study. *Journal of Geophysical Research: Oceans*, *123*, 3259–3285. https://doi.org/10.1029/2017JC013514

Received 28 SEP 2017
Accepted 12 APR 2018
Accepted article online 19 APR 2018
Published online 8 MAY 2018
Corrected 6 NOV 2018

This article was corrected on 6 NOV 2018. See the end of the full text for details.

Abstract The Taylor Energy Site is located in the vicinity of the Mississippi Delta region over the Northern Gulf of Mexico (NGoM). Surface oil patches have been persistently observed within this site since 2004, when an oil rig was destroyed by Hurricane Ivan. A multiplatform observational experiment was conducted in April 2017 to investigate, for the first time, the main hydrocarbon pathways from the Taylor Energy Site toward the NGoM continental shelves, and the Gulf interior, under the influence of local and regional physical processes. Results indicate that the Mississippi River (MR)-induced fronts over the Taylor Energy Site, in combination with local circulation, prevailing winds and broader regional dynamics determine the hydrocarbon transport. The drifters deployed during the field experiment, in tandem with satellite data, drone imagery, wind measurements, and radar-derived data, efficiently described three major hydrocarbon pathways, associated with MR plume dynamics (downstream/upstream coastal currents) and basin-wide circulation (offshore pathway). Two different types of drifters, drogued and undrogued, showed clearly different pathways, which suggest potential differences in the expected advection of oil, depending on whether it forms a surface slick or whether it is partially mixed below the surface. The existence of multiple river fronts influenced the fate of oiled waters, preventing the hydrocarbons from reaching the Delta, like a natural boom barrier, trapping and directing the oil either westward or eastward. Thermohaline measurements showed that the MR plume near Taylor was 5–10 m deep, while the clearer ocean was characterized by a 40 m upper ocean homogenous layer.

1. Introduction

The Northern Gulf of Mexico (NGoM) and especially the western and central region, around the Mississippi River (MR) Delta, is a major reservoir of oil and natural gas in the U.S. According to the U.S. Energy Information Administration, over 45% of total U.S. petroleum refining capacity and 51% of total natural gas processing plant capacity are located along the Gulf coast (https://www.eia.gov/special/gulf_of_mexico/). Oil leaks and accidents in the Gulf of Mexico (GoM), such as the explosion on the Deepwater Horizon (DwH) rig in 2010, have released significant quantities of hydrocarbons (Crone & Tolstoy, 2010; McNutt et al., 2012) in the sensitive marine environment around the MR Delta, and over the LouisianA TEXas (LATEX) and Mississippi Alabama FLoridA (MAFLA) shelves (Kourafalou & Androulidakis, 2013).

The aim of the current study is to investigate the main hydrocarbon pathways under the influence of the river plume dynamics, taking into account the broader mechanisms (both local and regional) forcing the NGoM circulation. We use multiplatform observations to detect and study the river-induced fronts, circulation patterns, water column characteristics, and surface oil patch distribution observed around the Taylor Energy Site, which is located very close to the MR Delta (Figure 1), approximately 17 km distance and at a depth of about 150 m. The study site is a natural laboratory of oil slicks interacting with riverine fronts. The Taylor Energy Site contains the now destroyed Taylor Energy oil rig. This rig was damaged in 2004 during the passage of Hurricane Ivan (Stewart, 2005) and since then surface oil slicks and sheens have been observed on the surface. Warren et al. (2014) showed that the surface oil patches over the Taylor Energy

© 2018. American Geophysical Union. All Rights Reserved.

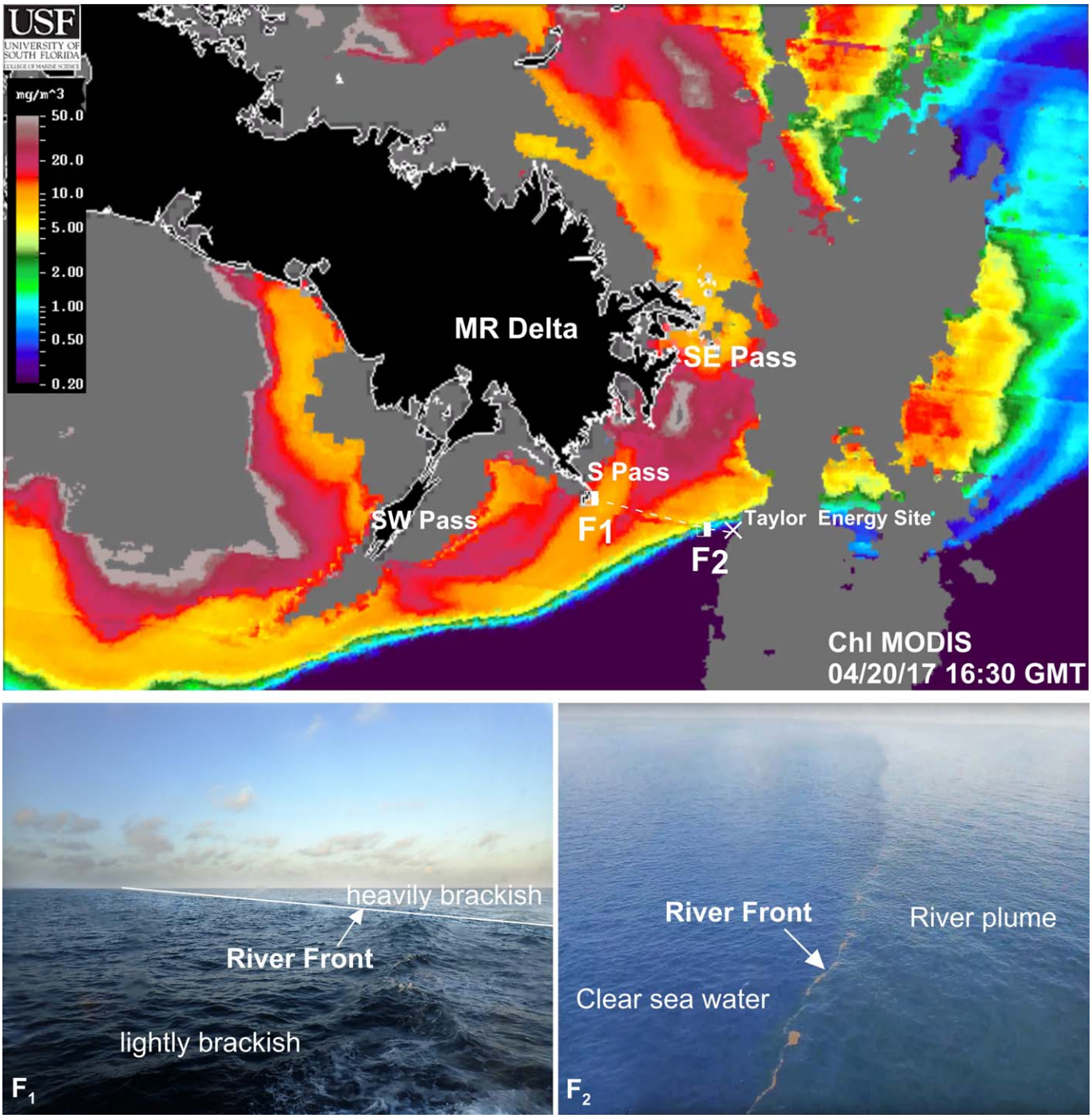

Figure 1. Ocean color image collected by MODIS (chl *a*; mg/m^3) on 20 April 2017 shows the river plume (high chl *a* content) spreading around the Mississippi River (MR) Delta indicating the inner (F_1) and outer (F_2) river fronts between the MR Delta and the Taylor Energy Site. The Southern (S), Southwestern (SW), and Southeastern (SE) Passes that release MR waters into the Gulf are shown. Images of the (low left) F_1 (from R/V St. Anthony) and (low right) F_2 (from Unmanned Aerial System, UAS) fronts, taken on 20 April 2017 are also presented. The river fronts are marked in both cases, separating heavily from lightly brackish waters (F_1) and the outer river plume boundary from clear sea waters (F_2). In the ocean color image, black represents land, dark grey represents clouds or other image artifacts, while light grey, dark red, and orange represent high chl *a* concentrations.

Site are frequently detected in satellite images (>130 oil reports between 2010 and 2014) and they are easier to be observed from April to October, due to the advantage of having sun-glint that peaks in detection in May and August–September (Hu et al., 2009). Our study area is unique, due to the long-term (~14 years)

existence of hydrocarbons in the vicinity of the strongest U.S. river discharge and over an ecologically sensitive region, especially after the disastrous DwH accident of 2010.

We concentrate on the fronts induced by the MR, one of the largest rivers in the world and the largest in North America, with an approximately historical average flow volume of 425 km^3/yr (Hu et al., 2005; Milliman & Meade, 1983). The riverine waters exit through several passes into NGoM (Figure 1), the largest ones being the Southwest Pass, South Pass, and Southeast Pass. The strong outflow discharge rates of freshwater via various passes around the Delta form an extensive plume of brackish waters with several successive density fronts between the high salinity open sea and the Delta (multiple fronts), as usually observed around large outflow rivers (Garvine & Monk, 1974). These frontal formations and the overall river plume evolution are controlled by changes in winds and discharge rates, especially during spring and early summer when the discharge rates usually increase (Androulidakis & Kourafalou, 2013; Walker et al., 1994). The topography and continental shelf morphology over the NGoM also attribute unique characteristics to the MR river plume patterns (Androulidakis et al., 2015; Schiller et al., 2011). During the observational campaign presented herein, a distinct front (F_1; Figure 1), separating waters with high chlorophyll *a* (chl *a*) concentrations and rich in sediments (heavily brackish) from waters with lower chl *a* concentrations (lightly brackish) within the plume, is formed near the South Pass on 20 April 2017. An outer strong front was also detected by both in situ measurements and ocean color images very close to the Taylor Energy Site (F_2; Figure 1). Large quantities of sargassum were observed along this front highlighting the distinct separation between two different water masses. These fronts are expected to play an important role on the transport of MR waters, as well as the transport of hydrocarbons over or near the NGoM shelf areas. We will examine transport pathways under the influence of rirverine fronts, broader shelf processes, and exchanges with offshore flows.

The major NGoM circulation patterns, especially over the central region, are determined by the MR discharge and the respective buoyancy-driven currents in tandem with wind conditions (Schiller et al., 2011; Walker et al., 1996, 2005). The buoyancy-driven MR plume waters have three distinct pathways that are common for large-scale rivers where the Coriolis effect is important (Garvine, 1995; Kourafalou et al., 1996): an anticyclonic bulge, around the MR Delta, a "downstream" coastal current in the direction of Kelvin wave propagation toward the LATEX shelf and an "upstream" current toward the MAFLA shelf (Androulidakis & Kourafalou 2013; Kourafalou & Androulidakis, 2013; Schiller et al., 2011; Schiller & Kourafalou, 2014; Walker, 1996; Walker et al. 1996). Morey et al. (2003), based on numerical simulations, showed that the westward and eastward propagation of the river plume waters reveal a clear seasonality: eastward in the spring/summer and westward in the fall/winter. The river discharge rates, the wind state, the local dynamics, and the regional circulation features may alter the typical buoyancy-driven patterns and moreover affect the plume spreading, its vertical structure, and front location (Androulidakis et al., 2015; Androulidakis & Kourafalou, 2013; Schiller et al., 2011; Schiller & Kourafalou, 2014; Walker et al., 2005). Downstream westward and upstream northeastward currents of the river plume are enhanced by easterly (downwelling-favorable) and westerly (upwelling-favorable) winds, respectively (Androulidakis et al., 2015; Schiller et al., 2011; Walker et al., 1994, 2005).

The exchanges of NGoM shelf waters with regional offshore flows are governed by the Loop Current (LC; a branch of the Gulf Stream) and its associated eddy field. The LC system may facilitate the offshore removal of riverine waters toward remote Gulf areas (Androulidakis & Kourafalou, 2013; Le Hénaff & Kourafalou, 2016; Schiller et al., 2011; Schiller & Kourafalou, 2014), as well as the offshore transport of surface oil toward the Gulf interior (Hamilton et al., 2011; Le Hénaff et al., 2012a; Walker et al., 2011). The offshore removal of brackish waters under the LC system influence has been observed to reach the southern GoM areas and even the Atlantic Ocean (Hu et al., 2005; Ortner et al., 1995). The LC extension toward the NGoM, especially north of 28°N, the changes associated with the shedding of an anticyclonic ring (LC Eddy, LCE), and the cyclonic LC Frontal Eddies (LCFEs) that also play a role in the LCE shedding process (Le Hénaff et al., 2012b), contribute to the circulation over our study area.

We seek to investigate whether oil is trapped along the riverine fronts, what processes control the frontal alignment of oil pathways and how such entrapment may influence the overall transport and fate of the hydrocarbons. The MR-induced circulation modified by shelf and slope flows, was found to substantially influence the near-surface transport of oil during the DwH period (Falcini et al., 2012; Kourafalou & Androulidakis, 2013). Based on hydrodynamic simulations and observations, Kourafalou and Androulidakis (2013)

showed that the MR plume buoyancy-driven effects on the DwH oil transport had different aspects for east and west of the MR Delta. Although several other atmospheric and oceanic conditions mainly determined the oil spill fate (Le Hénaff et al., 2012a; Walker et al., 2011), the river plume buoyancy-driven contribution was vital to the spreading of the DwH hydrocarbons over the central NGoM. These modeling studies suggested that the river-induced fronts could be an important factor in determining the fate of the hydrocarbons (our main study hypothesis), motivating an observational approach.

We conducted a multiplatform field experiment in April 2017 to examine, for the first time, major pathways of oiled waters originating from areas around the Taylor Energy Site under local and regional physical processes, such as the formation of density fronts, wind-driven circulation and regional dynamics (LC and eddies). Different types of drifters were deployed in order to capture various effects (e.g., winds, currents, and buoyancy) on the hydrocarbon pathways. This study extends drifter experiments in relation to oil spills that were conducted in the GoM in the past (Liu et al., 2011; Price et al., 2006; Smith et al., 2014). More than 300 satellite-tracked near-surface drifting buoys were deployed in the NGoM as part of the Grand Lagrangian Deployment (GLAD) expedition (Berta et al., 2015; Mariano et al., 2016; Olascoaga et al., 2013; Poje et al., 2014). Our study was unique, as it combined drifter launches with multisensor high-resolution satellite imagery covering the period of field operations, drone flights, marine radar observations, and in situ thermohaline measurements collected around the Taylor Energy Site. In addition to the overarching objective to explore the pathways of oiled waters and to document how they were influenced by the river-induced fronts (in the context of other circulation characteristics), we sought to examine how the spreading of oil slicks is influenced by the variability in oil thickness.

More information about the observational platforms, methods, and data is given in section 2. Section 3 presents the major surface transport pathways revealed from the drifter data (section 3.1). This section also discusses the local dynamics, especially the variability of river fronts (section 3.2.1) and the surface circulation (section 3.2.2). Section 4 contains the regional circulation effects on hydrocarbon pathways (section 4.1), the vertical upper ocean structure in the study area (section 4.2), and the observed patterns of the oiled waters spreading (section 4.3). Finally, a summary of concluding remarks is presented in section 5.

2. Data and Methods

The multiplatform observations include several drifter deployments, shipboard radar sea-surface roughness imagery, thermohaline measurements from R/V Walton Smith, drone imagery, and satellite data. The field experiment took place on 18, 20, and 25 April 2017, while the drifters continued to report their positions through May and early June.

2.1. Drifter Measurements

A total of 14 GPS-Tracked drifters were deployed from research vessels within the Taylor Energy Site study area (approximately at 88.97°W, 28.93°N). Each drifter's original name (drifter ID) and the respective number (drifter #) assigned for the purposes of the study are presented in Table 1. The drifter trajectories served the main goal of the study to describe pathways of hydrocarbons pathways released at the Taylor Energy Site. They were also used to follow the flow in both the surface and upper meter (subsurface) in order to distinguish between advection of surface slicks and oil mixtures within the upper layer of the water column. We employed two types of drifters (drogued and undrogued), as we wanted to follow surface material pathways (like oil slicks) and distinguish them from possible subsurface (∼0.5 m below surface) material pathways (like oil droplets suspended in the upper meter). By using these two types of instruments, we could examine if the presence (absence) of drifter drogue had an impact on following subsurface (surface) transport of oil. We assume that the river plume is deeper than the drogue depth and, therefore, the drogued drifters are also influenced by the plume and the respective density fronts.

The Norwegian Meteorological Institute (https://www.met.no) provided 2 MetOcean (http://www.metocean.com) drifters. The Consortium for Advanced Research on Transport of Hydrocarbon in the Environment (CARTHE; http://carthe.org) provided 12 drifters that they have designed as a prototype for the GoM studies (Lumpkin et al., 2017; Novelli et al., 2017). Two different types of MetOcean drifters were deployed on 18 April, the undrogued (UN) I-Sphere and the drogued (DR) Code/Davis (from here on referred to as Davis). The I-Sphere (UN1; Table 1) has a spherical shape and is specifically designed to track oil spills at the surface.

Table 1
Drifters Names, Dates, Type, and Trajectory Color Used in Maps

Drifter ID	Drifter #	Launch date and time (GMT) [distance from front]	End date (coastal landing)	Type	Color in maps
I-Sphere	UN1	18 Apr 16:30 [∼6 km, onshore]	21 Apr (90.83°W–29.04°N)	Undrogued	Black
Davis	DR1	18 Apr 23:28	10 May	Drogued	Green
T1_0275	DR2	18 Apr 16:41 [∼6 km, onshore]	11 May	Drogued	Magenta
T1_0088	UN2	18 Apr 16:41 [∼6 km, onshore]	21 Apr (90.84°W–29.08°N)	Undrogued	Blue
T1_0092	DR3	20 Apr 12:48	27 Apr	Drogued	Magenta
T1_0321	UN3	20 Apr 12:48	29 Apr (90.76°W–29.12°N)	Undrogued	Green
T1_0109	UN4	20 Apr 14:00	22 Apr (90.18°W–29.11°N)	Undrogued	Black
T1_0107	DR4	20 Apr 14:00	17 May	Drogued	Green
T1_0083	UN5	20 Apr 16:30 [<1 km, offshore]	27 Apr (90.01°W–29.22°N)	Undrogued	Blue
T1_0501	DR5	20 Apr16:30 [<1 km, offshore]	20 May	Drogued	Purple
T1_0513	DR6	25 Apr 20:35 [∼25 km, onshore]	09 Jun	Drogued	Black
T1_0487	DR7	25 Apr 20:38 [∼25 km, onshore]	30 Apr (88.65°W–30.56°N)	Drogued	Green
T1_0112	UN6	25 Apr20:38 [∼25 km, onshore]	17 May	Undrogued	Purple
T1_0167	DR8	25 Apr20:40 [∼25 km, onshore]	29 Apr	Drogued	Magenta

Note. The coordinates of the drifters that landed on the coast are given (in parentheses). The deployment's distance and position (offshore or onshore) from the outer river front (0.25 mg/m^3), derived from the ocean color images (MODIS) if available near the time of the drifter deployment is also presented (in brackets).

It is about 50% submerged and is hence subject to wind drift, Stokes drift and surface currents (Röhrs et al., 2012). The Davis (DR1; Table 1) drifter is designed to acquire ocean currents near the surface, with a drogue at about 70 cm below the surface (Röhrs & Christensen, 2015). Only the antenna is above the surface, and consequently its design promotes a low wind-induced slip and a good representation of the current averaged over the upper 1 m (Davis, 1985). Both types of MetOcean drifters transmit their GPS position every 30 min via the Iridium network. The compact, biodegradable CARTHE drifters (Novelli et al., 2017) are composed of a donut-shaped float at the surface, which contains the GPS and battery unit, and a tethered submerged drogue, made of two perpendicular bio-plastic panels, with a center of mass at ∼40 cm below the surface. This drogue can be removed, in which case the drifter is only composed of the surface donut-shaped float and thus referred to as undrogued drifter. The GPS transmitter is produced by Globalstar (SPOT Trace) and powered by D-cell Alkaline batteries, yields an average of 60 days of GPS position fixes at 5 min resolution. Both drogued and undrogued CARTHE drifters were extensively calibrated in the laboratory and in the field, to accurately follow the Lagrangian currents across the upper 0.60 and 0.05 m, respectively. Drogued drifters show a reduced wind-induced slip velocity of less than 0.5% of the neutral wind speed at 10 m. In field experiments, their velocity matched that of nearby Davis drifters to an accuracy of 2 mm/s. The undrogued CARTHE drifters show a higher wind-induced slip velocity 2% or less of the neutral wind speed at 10 m for wind speeds ranging from 8 to 23 m/s. The difference in drift between the undrogued CARTHE drifter and the MetOcean I-Sphere has not been investigated yet, but both drifters can be expected to respond more to wind-induced and wave-induced surface currents, presumably like oils slicks would, with respect to deeper subsurface currents. Two pairs of drogued and undrogued drifters were deployed from the R/V Saint Anthony at the Taylor Energy Site during the first day of the experiment (18 April; Table 1). Six more CARTHE drifters (three drogued, three undrogued) were deployed on 20 April; two drogued-undrogued pairs were deployed inside the range of the marine radar installed on the R/V Walton Smith (see section 2.2.1), which had joined the experiment early in the morning of 20 April. The last deployment of four CARTHE drifters (three drogued, one undrogued) took place at the Taylor Energy Site on 25 April under different wind conditions (see section 3.1).

2.2. Ship-Borne Observations

2.2.1. Marine Radar Current Mapping

Marine radars have been shown to be very useful for oceanographic remote sensing purposes (Horstmann et al., 2015). A coherent-on-receive marine X-band (9.5 GHz) radar (Braun et al., 2008), developed at Helmholtz Zentrum Geesthacht (HZG), Germany, was installed on the R/V Walton Smith to support this study. HZG radar data were collected from the ship over the Taylor Energy Site on 20 April 2017. The radar was operated with a rotating antenna and grazing incidence, where the backscatter of the ocean surface is

primarily caused by the small-scale surface roughness (∼1.5 cm). Ocean waves that are longer than two times the radar resolution become visible due to tilt and hydrodynamic modulation of the surface roughness and geometrical shadowing, all caused by longer waves. Using a 3-D fast Fourier transform, a radar images sequence is converted to the wave number-frequency domain where the surface wave energy is located on an inverted cone (the so-called dispersion shell), which is perfectly circular in the absence of currents (Young et al., 1985). Any deviation from this circular form is due to the Doppler term in the linear dispersion relationship. An iterative least squares fit technique is employed to find the near-surface current vector that minimizes the distance between the wave signal and the dispersion shell (Senet et al., 2001). For shipboard installations, care must be given to the ship motion correction, since even slight offsets in the orientation of the radar images may lead to significant cross-track errors in the current estimates (Lund et al., 2015). To obtain near-surface current maps, the above analysis is performed within circular analysis windows that have a ∼475 m radius and are evenly distributed over the radar field of view, resulting in an error below 0.04 m/s (Lund et al., 2018). The marine radar mapping technique was validated with more than 4,000 radar-drifter pairs in a previous experiment in the GoM. The marine radar near-surface current maps are presented together with the corresponding 2 min averaged backscatter intensity images. The radar backscatter intensity images show submesoscale current features that modulate the sea-surface roughness (e.g., frontal convergence zones). They also show oil slicks as they dampen the sea-surface roughness.

2.2.2. Temperature and Salinity Measurements

On 20 April 2017 (15:10–17:02 GMT) the R/V Walton Smith performed two transects across the MR front and near the Taylor Energy Site, where a Conductivity-Temperature-Depth (CTD) cast also took place. The location of the sections was carefully selected to avoid any accidental clogging of the different water sampling systems from the oil slick. The first transect was directed onshore on a northwestward direction and the second one backtracking offshore along the opposite direction. The vertical CTD cast down to 110 m depth was completed first. Surface temperature and salinity were measured continuously (1 Hz) during the entire duration of both transects via a hull-mounted flow-through system 1.5 m below the ship's waterline using a ThermoSalinoGraph (TSG) Sea Bird Electronics (SBE) 21 SeaCat. Additionally, an Acrobat undulating towed vehicle (Sea-science) fitted with a SBE 49 Fast Cat CTD was deployed behind the ship throughout both transects. The Acrobat was set to undulate from the surface to a maximum depth of approximately 48 m at a targeted mean speed over ground of 1.5 m/s.

2.3. Satellite Data and Aerial Imagery

Data sets and images from several satellites are also part of the multiplatform observations. The first data set includes daily and 7 day mean chl *a* concentration images (in mg/m^3) in the surface ocean layer, derived from the MoDerate resolution Imaging Spectroradiometer (MODIS) Aqua (Hu et al., 2012). Images from two satellite products were used from this data set to detect the river plume evolution and identify the multiple fronts of the plume and especially the outer front with the clear ocean waters with respect to chl *a* concentrations. The first product covers the MR region with more detail and the second one includes the broader NGoM region. The second data set is from the Group for High Resolution Sea Surface Temperature (GHRSST), which includes gridded Sea-Surface Temperature (SST) fields. We use the GHRSST Level 4 SST fields (produced by GHRSST daily Level 2 data; Donlon et al., 2009), covering the GoM region with horizontal resolution of 1–2 km. These SST fields are employed to investigate local temperature changes associated with the MR the waters and the regional circulation patterns (LCFEs, LC, and LCEs; see section 4.1). The third satellite data set is the Archiving, Validation and Interpretation of Satellite Oceanographic (AVISO) data. These data include the Sea Level Anomaly (SLA) estimated with altimeters in orbit. Maps of Absolute Dynamic Topography (MADT) were computed from the respective SLA fields by adding the Mean Dynamic Topography that is also part of the AVISO database. The satellite MADT fields were used to investigate the offshore pathways under regional circulation effects in tandem with the drifters, GHRSST and chl *a* data (see section 4.1).

In collaboration with National Oceanic and Atmospheric Administration (NOAA) and MacDonald-Dettwiler and Associates (MDA), a number of satellite images were acquired during our field operations. Microwave Synthetic Aperture Radar (SAR) imagery were collected by RADARSAT-2 (20 April), TerraSAR-X (26 April), and Sentinel-1 (28 April). SAR imagery is well known for its capacity to detect oil under a wide range of wind speeds and regardless of the illumination conditions (Garcia-Pineda et al., 2009, 2013). Floating oil slicks produce distinctive signatures on SAR images. When the small-scale sea-surface roughness is dampened or

smoothed by viscoelastic properties of an oil slick or any other surfactant, less incident energy from the SAR spacecraft is backscattered to the sensor, reducing radar backscatter. The oil-covered areas usually have distinctly contrasting brightness against the radar backscatter produced by wind-generated ripples. The visual differences among the SAR data are based on the specific configuration of the SAR sensors including: wavelengths, incidence angle, polarization, spatial resolution, noise floor, and instrument noise. While the RADARSAT-2 image was collected at C-Band in fully polarimetric mode, Sentinel-1 and TerraSAR-X (C-Band and X-Band respectively) images were collected in single polarization mode. In addition, MODIS Terra Red-Green-Blue (RGB) image (25 April; see Figure 12a) is used to identify potential oil slicks (Hu et al., 2009). Two additional images were collected on 25 April by the Advanced Spaceborne Thermal Emission and Reflection Radiometer (ASTER) instrument on NASA's Terra spacecraft (resolution 15 m) and by Worldview-2 multispectral satellite with an approximate spatial resolution of 1.5 m. The ASTER's passive sensor has 14 spectral bands from the visible to the thermal infrared wavelength region. Thick and thin oil patches are clearly visible in such images by enhancing the RGB bands. The Worldview-2's high resolution allows to identify not only features related to thick oil on high detail but also shows the suspended matter contrast of the MR plume compared to the clear water from the GoM.

An Unmanned Aerial System (UAS) was also used as part of the measurements over the Taylor Energy Site. The UAS imagery provides an efficient way to navigate the boat to strategic areas over the oil slick. A real-time video broadcast system is used to observe the conditions of the oil and river front from an aerial perspective. The UAS system allowed us to monitor the oil and to position the vessel in a tactical way for the deployment of the drifters. Figure 1 shows an aerial view from the UAS at 120 m altitude.

2.4. Wind and River Discharge Data

Wind measurements, collected by three National Data Buoy Center (NDBC) buoys were used to describe the wind conditions over the NGoM during the field experiment. Buoy SPLL1, owned and maintained by Coastal Studies Institute, Louisiana State University, is located west of the Delta and over the LATEX shelf (28.867°N, 90.483°W). The northeastern region is represented by buoy 42012, located close to the coast over the central MAFLA continental shelf (30.064°N, 87.551°W). The wind conditions of the offshore area, south of the Taylor Energy Site, are described by buoy KIKT, located at Mississippi Canyon 474 (28.521°N, 88.289°W). The measurements from these three buoys are used to show potential differences/similarities of the wind state between the downstream (SPLL1), upstream (42012), and offshore (KIKT) regions in respect to the river plume spreading. In addition, 3-hourly wind data were derived from the Navy Global Environmental Model (NAVGEM) at the Taylor Energy Site (where drifters were deployed), due to the absence of available observations. These four time series from different regions also serve to examine if the wind state over the central NGoM was generally homogenous during our study period. Daily MR discharge rates, measured at Tarbert Landing by the US Army Corps of Engineers are used to describe the freshwater input during the experiment (April–May); climatological rates are used for comparison.

3. Results

The multiplatform observations are analyzed and combined to offer a synthesized view of the general pathways of hydrocarbons originating around the Taylor Energy Site, under the influence of river-induced fronts. The drifter data are the major tool to determine the transport and fate of oiled waters, while the detection of the multiple river fronts and their role on spreading the oil, especially during the early hours after the deployments of the drifters, is supported by the satellite imagery and the measurements (radar and thermohaline) by the R/V Walton Smith.

3.1. Hydrocarbon Pathways Revealed From Drifter Data

Drifter names and characteristics are given in Table 1. The overall drifter trajectories after the three deployment dates of April 2017 and selected ocean color snapshots during the propagation of the drifters are presented in Figure 2. The respective MR discharge and wind conditions over NGoM are presented in Figure 3. They reveal effects of the wind evolution, the river plume spreading, and the local circulation patterns on the drifter trajectories, which represent the potential hydrocarbon pathways over the broader Delta region.

3.1.1. Deployments on 18 April

The drifters were deployed inside the river plume, approximately 6 km north of the outer front, during the first day of the field experiment (18 April, Table 1). The initial pathway of all four drifters was westward, over

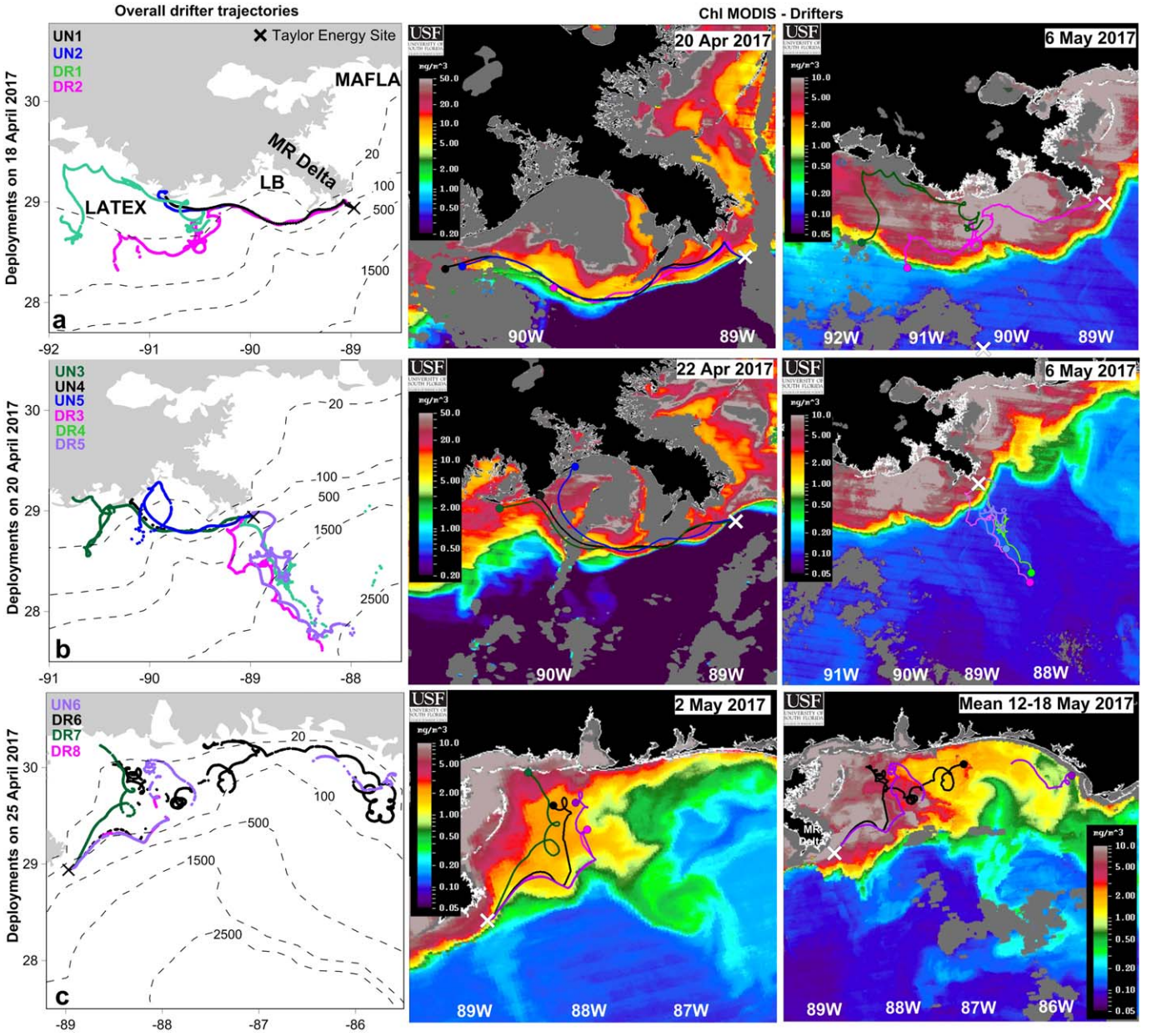

Figure 2. Overall drifter trajectories and ocean color (chl *a* concentration; MODIS) snapshots from the (a) 18 April, (b) 20 April, and (c) 25 April deployments. Trajectory colors correspond to the drifter names (details in Table 1). (left) The full drifter trajectories (periods in Table 1) and (middle and right) the trajectories up to the date of each MODIS image (dates at the top of each figure). Different types of drifters (drogued and undrogued; Table 1) were used to describe the evolution of oil patches with various thicknesses originated from around the Taylor Energy Site (indicated with cross symbol). Dashed lines indicate the 20, 100, 500, 1,500, and 2,500 isobaths. The Louisiana Bight (LB), the Mississippi River (MR) Delta, the Louisiana-Texas (LATEX), and the Mississippi-Alabama-Florida (MAFLA) shelves are marked in Figure 2a. In the ocean color images, black represents land, dark grey represents clouds or other image artifacts, while light grey, dark red, and orange represent high chl *a* concentrations.

the Louisiana Bight (LB, Figure 2a). Both undrogued drifters (UN1 and UN2) followed a nearly identical pathway, passed the LB by 20 April and landed on the coast west of the Delta at ~91°W around 21 April (Table 1). The drogued DR2 drifter followed a similar path with lower speed (see section 3.2) over the LB but remained active for a longer period, without landing on the coast. Both drogued and undrogued drifters followed the MR downstream current (waters of high chl *a* concentrations) along the front between the brackish river waters and the ocean masses clearly visible in Figure 2a (Columns 2 and 3).

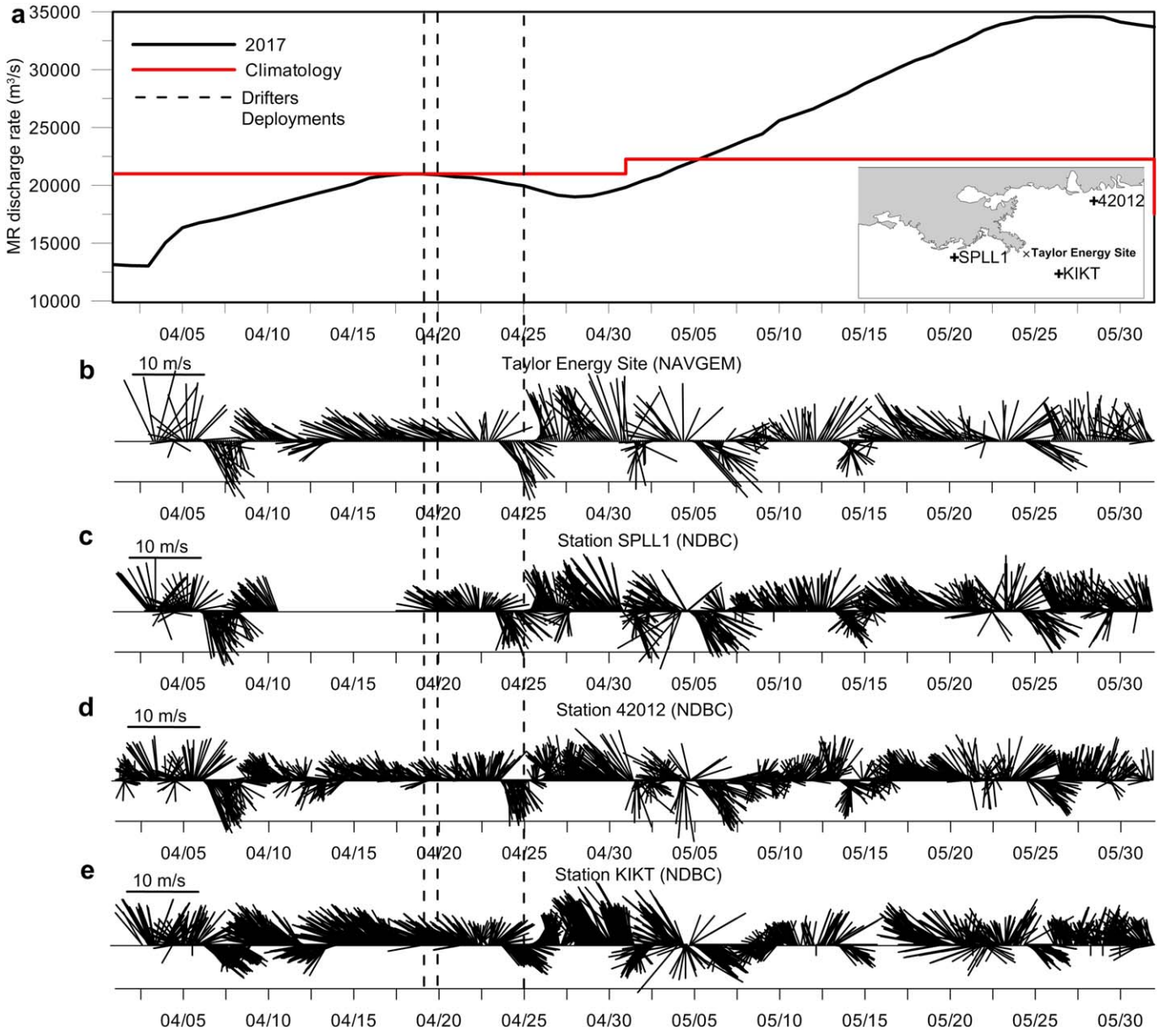

Figure 3. (a) Evolution of Mississippi River (MR) daily discharge (m^3/s) during April–May 2017 (black line) and the respective climatological monthly rates (red line). Evolution of wind vectors from the simulation of (b) Navy Global Environmental Model (NAVGEM) at Taylor Energy Site, and National Data Buoy Center (NDBC) measurements at (c) Station SPLL1, (d) Station 42012, and (e) Station KIKT during April–May 2017. The dates of drifter deployments at the Taylor Energy Site are indicated with dashed lines. The locations of the Taylor Energy Site and NDBC buoys are marked in the insert of Figure 3a.

The downstream current usually forms an anticyclonic circulation pattern over the LB that may drag surface waters toward the coast in the west part of the Bight in agreement with an older study by Wiseman et al. (1975) and more recent findings by Androulidakis et al. (2015; their Figure 3). This pattern, in combination with the southeasterly winds observed over the LATEX shelf (SPLL1; Figure 3c), narrowed the downstream plume west of the LB and allowed the faster undrogued drifters to approach the coast by 20 April and finally land on the beach one day later. All three meteorological buoys recorded persistent southeasterly winds, confirming that the wind field was homogenous over the entire study region, in agreement with previous studies in this area (i.e., Schiller et al., 2011; Walker et al., 2005). Although buoys SPLL1 and 42012 are significantly distant from one another, located in the western (LATEX) and eastern (MAFLA) NGoM continental shelves, respectively, the variability of the wind speed and direction is almost identical (Figure 3). The wind evolution derived from the NAVGEM model at the Taylor Energy Site shows a similar variation, with

strong southeasterly winds (~10 m/s; Figure 3b) during the first two deployment dates (18 and 20 April 2017). The large quantities of brackish waters along the downstream current are due to a combination of an increasing trend of the river discharge from below climatology to close to 20,000 m^3/s after mid-April (Figure 3a) and the prevailing strong easterly winds over the area. Both environmental conditions strengthen the westward downstream current (Androulidakis et al., 2015; Walker et al., 1994), carrying large quantities of low salinity waters across the LB and along the LATEX shelf.

The slower drogued drifter DR2 reached the same region of LB and moved toward the coast on 21 April. The drifter was then carried offshore, over the outer river front, as presented on 6 May (Figure 2a). This offshore displacement followed the widening of the downstream current region, which is clearly shown between the two ocean color images on 20 April and 6 May, when the plume is significantly wider along the western coasts (Figure 2a). This change from a narrow, buoyancy-driven westward coastal current to an offshore advection of brackish waters is generally due to upwelling-favorable (westerly) winds, in agreement with Androulidakis et al. (2015). Indeed, a period of westerly winds was observed between 23 and 26 April. This effect was short lived, as the last two weeks of April were mainly dominated by easterly and southeasterly winds. The first drogued drifter (DR1) that started emitting on 23 April, although it was launched on 18 April, was also located at the outer river plume front on 6 May. The southward turn of this drifter took place on 4 May, when the winds again began to change from easterlies to southwesterlies (Figure 3c). Its southward offshore propagation is similar to the DR2 drifter, also related to the offshore shift of the front at the end of April and in the beginning of May during the second period with strong westerly winds (>10 m/s). Both drogued drifters showed a similar southward turn, in tandem with the change in the wind direction around 5 May, but in different locations of the river plume: the DR2 approached 91.25°W over the 20 m isobath and the outer plume front, while the DR1 was closer to the coasts at 92°W.

3.1.2. Deployments on 20 April

Six drifter deployments took place at the Taylor Energy Site on 20 April (Figure 2b and Table 1). The three undrogued drifters (UN3, UN4, and UN5), influenced by easterly wind-induced surface currents (Figure 3b), had trajectories along the MR front by the downstream current toward the west. They were trapped into the anticyclonic bulge over the LB and finally were washed out at 90°W on 22 April, before the wind direction change on 23 April. The prevailing southeasterly winds between 20 and 22 April (Figure 3c) determined this pathway, driving the surface waters along the outer plume front and finally toward the coast, west of the LB. It is noted that all undrogued drifters deployed on 18 and 20 April propagated westward along the front and their fate was largely determined by the extension of the plume and thus the front's location under the effect of strong easterly winds.

The drogued drifters DR3 and DR4, deployed in the morning of 20 April (Table 1), initially moved northward toward the river plume and then westward along the plume front. However, because of their slower speed, they stayed longer in that area. The change in the wind direction after 23 April (Figure 3b) affected their propagation which turned toward the south in contrast to the undrogued drifters that rapidly moved westward before the wind change from easterly to southwesterly. The wind started changing direction on 23 April and became westerly by 25 April. The outer plume front was north of the Taylor Energy Site at a close distance (<1 km; Table 1) in the morning of 20 April (Figure 4b), in contrast to its position two days earlier (18 April), when the deployment area (Taylor) was totally inside the plume (Figure 4a). Similarly, the drogued drifter DR5 that was deployed on 20 April (Table 1) followed the same offshore pathway as the other two drifters. The main pathway described by the three drogued drifters deployed on 20 April was toward the central Gulf, following a narrow offshore branch of low salinity waters observed in the ocean color image on 6 May (~0.20 mg/m^3; Figure 2b). Measurements at the offshore KIKT buoy (Figure 3e) showed that winds changed direction again (from eastward to northward) during the period from 27 April to 4 May, without affecting the major southward track of the drogued drifters, which were mainly influenced by the ocean currents related to mesoscale eddy circulation (see section 4.1).

3.1.3. Deployments on 25 April

The final deployment of drifters at the Taylor Energy Site took place in the afternoon of 25 April, when the river plume was extended over the area (Figure 2c and Table 1). Westerly upwelling-favorable winds prevailed during the deployments (Figure 3b), while the MR outflow rates were slightly lower than the climatology levels of April. All drifters propagated northeastward, following the enhanced upstream coastal current, carrying significant quantities of brackish waters toward northeast of the Delta and over the MAFLA continental shelf (Figure 2c). A significant trend of the MR discharge increase was observed during May

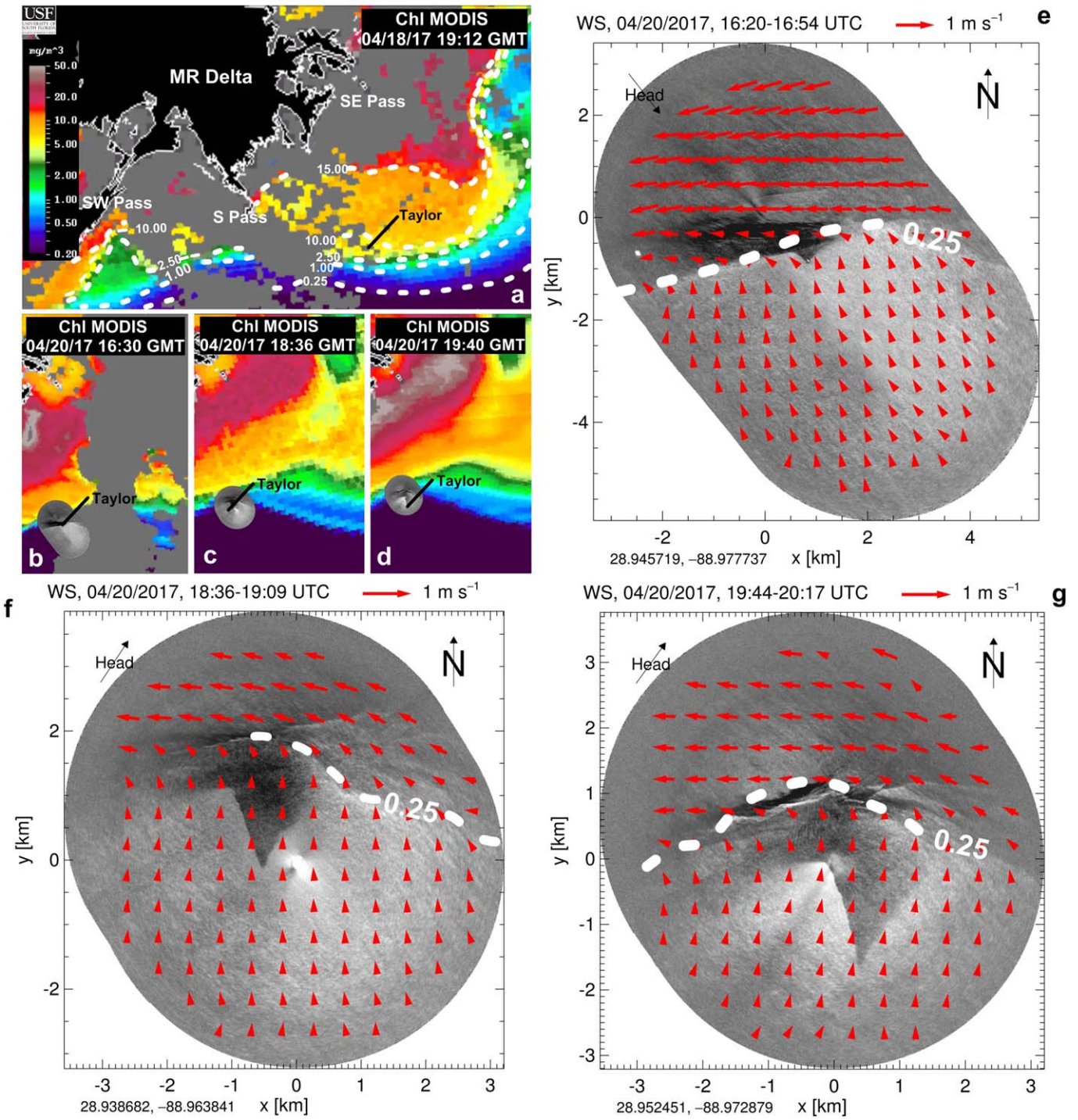

Figure 4. Distribution of MODIS chl *a* concentrations (mg/m^3) on (a) 18 April 2017 04:35 GMT, (b) 20 April 2017 16:30 GMT, (c) 20 April 2017 18:36 GMT, and (d) 20 April 2017 19:40 GMT around the Mississippi River (MR) Delta. The dashed lines indicate several contours (0.25, 1.00, 2.50, 10.00, and 15.00 mg/m^3) of chl *a* concentration representing the respective fronts of the MR plume. The location of the Taylor Energy Site is also marked. The Southern (S), Southwestern (SW), and Southeastern (SE) Passes of MR are shown. Three successive radar imagery snapshots (e–g) contain the related surface currents (red vectors) measured over an area (∼3 km radius) around the R/V Walton Smith with respect to the three chl *a* maps (b–d) from the second day of the field experiment (20 April 2017; no radar measurements are available on 18 April 2017). The dark grey areas in background are characterized by oiled waters and the dashed line indicates the 0.25 mg/m^3 derived from the MODIS chl *a* concentrations. The direction (head) of the ship in each case is marked as "Head" (black arrow). In the ocean color image, black represents land, dark grey represents clouds or other image artifacts, while light grey, dark red, and orange represent high chl *a* concentrations.

(Figure 3a), leading to a strong peak by the end of May (~35,000 m^3/s), much higher than the climatological mean values of May (~21,000 m^3/s). The undrogued UN6 and the two drogued drifters (DR6 and DR8) followed the river plume front along the 100 m isobath until 88°W and finally revealed a similar northeastward pathway across the shelf until 2 May. The trajectory of the drogued DR7 drifter was more to the north, resulting in a coastal landing at the western MAFLA (~88.5°W) on 30 April (Table 1). The difference between these two pathways is related to a difference in the initial propagation of the drifters during the first day after their deployment (26 April) and the position of the successive fronts within the river plume (see section 3.2). The second peak of northwesterly winds after 4 May contributed to the enhancement of the upstream coastal current in combination with the MR outflow increase. This northeastward flow advected large quantities of brackish waters over the entire MAFLA shelf. This major pathway was efficiently traced by both DR6 and UN6 drifters, which reached the eastern part of the shelf by the end of May. The undrogued UN6 was already located over the eastern NGoM by 13 May, when southwesterly winds were still dominant along the MAFLA shelf (Figure 3d). This pathway showed that the surface waters, which can be contaminated with hydrocarbons in the case of large-scale oil spills (e.g., DwH accident), might spread along the eastern NGoM continental shelf and even reach the northwestern coasts of Florida.

3.2. Local Dynamics

The local circulation and thus the initial pathways of the Taylor Energy Site hydrocarbons are strongly related to the river plume patterns. The extension of the brackish plume and the location of the fronts between the lower (riverine) and higher (ocean) salinity water masses are strongly related to the prevailing winds, discharge rates, and the ocean currents. Therefore, the location and characteristics of the river plume fronts with respect to the Taylor Energy Site may contribute to the fate and pathways of the hydrocarbons. The major multiple fronts derived from the satellite chl *a* distribution are marked in Figure 4a.

3.2.1. Variability of River Fronts

The Taylor Energy Site was located inside the river plume between the chl *a* contours of 10 and 2.50 mg/m^3, 6 km north of the outer front (0.25 mg/m^3), on 18 April (Figure 4a). A higher chl *a* contour (15 mg/m^3) was located close to the tip of the South Pass, indicating another strong river front. The initial propagation of the drifters, deployed on 18 April under easterly winds, took place inside this high chl *a* water mass. They initially moved northeastward over a short distance (barely seen on Figure 2a), then they were trapped and aligned with the 15 mg/m^3 front (Figure 2a). The drifters propagated along the front and toward the west after 19 April.

The outer front of the MR plume (0.25 mg/m^3) was located in the vicinity of the Taylor Energy Site on 20 April. The marine radar image taken at the Taylor Energy Site confirmed that the river-induced front was located very close and north of the oil-covered area (Figure 4b). This indicates a noticeable onshore shift of the plume between the first deployment day (18 April) and the second deployment day (20 April) day of drifter deployments. The location of the river-induced front in the morning of 20 April is also detected by the TSG (R/V Walton Smith) measurements presented in Figure 5. Salinity changes from 36 to 28 took place within only 7 km, while the ship moved across the front along both S_1 and S_2 sections. The SST also increased on the river plume side of the front, as the ship encountered the low salinity waters. However, the surface differences in temperature are relatively small (<0.6°C) compared to the salinity ones that are very large (~8), indicating that the density front was mainly controlled by salinity changes between the brackish river plume and the open ocean waters. The persisting easterly winds (downwelling-favorable) during these two dates (18 and 20 April) presumably caused the observed northwestward shift of the plume. The outer river-induced front was located exactly at the Taylor Energy Site one day before, on 19 April (not shown). Based on idealized numerical experiments, Androulidakis et al. (2015) showed that easterly winds might reduce the radius of the anticyclonic bulge of the plume and promote the onshore shift of the front around the Delta, enhancing the advection of brackish waters directly toward the LATEX shelf.

The onshore shifting of the river plume was clearly seen on 20 April (Figures 4c and 4d). The marine radar image starting at 18:36 GMT (Figure 4f) coincides with the respective ocean color image (Figure 4c), both showing the outer river front located north of the Taylor Energy Site. Northward weak currents prevailed outside the plume, while stronger westward downstream currents are apparent north of the 0.25 mg/m^3 front. In section 3.1, we showed that the two drogued drifters DR3 and DR4 released on 20 April finally moved offshore toward the south, although their initial pathway was along the 0.25 mg/m^3 front, similar to the undrogued ones. Both drifters initially moved northward, following the weak northward currents, and

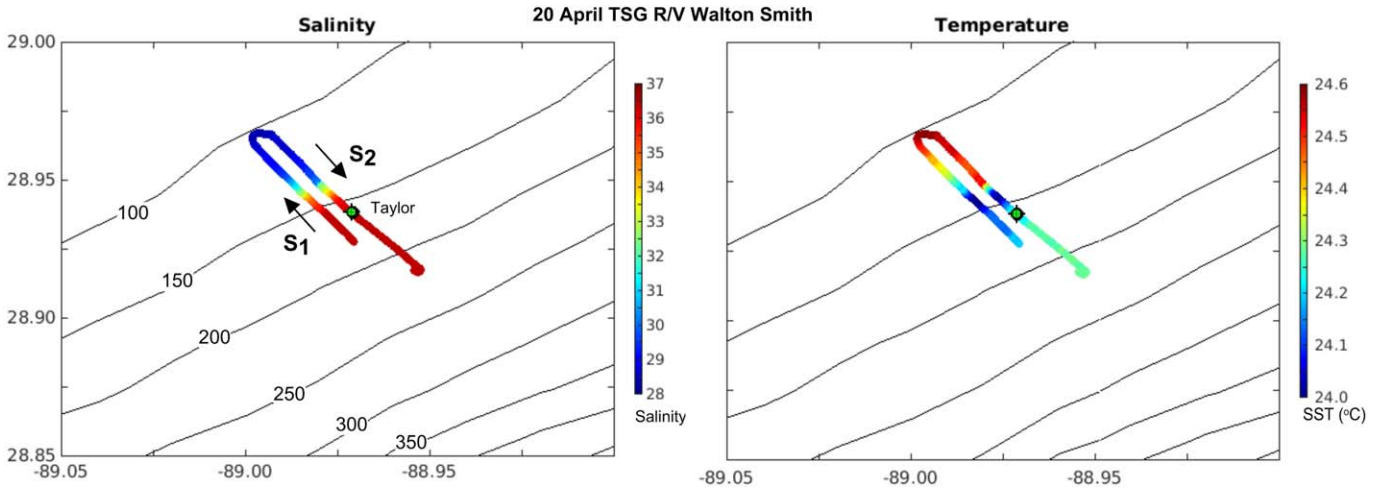

Figure 5. Distribution of Sea-Surface Temperature (SST; °C) and surface salinity measured by the ThermoSalinoGraph (TSG) on board the R/V Walton Smith along the cruise track over the Taylor Energy Site on 20 April. Contours indicate isobaths every 50 m and arrows show the direction of the ship route along sections S_1 and S_2.

then they were trapped in the plume front, located 2 km north of the Taylor Energy Site, a few hours after their deployment on 20 April. An oil patch moving from Taylor to the river front was captured by the marine radar image (Figure 4f), showing a similar northward pathway of hydrocarbons that was not so apparent earlier that day, when the front was very close to Taylor (Figure 4e). The distance between Taylor and the plume front increased even more 1 h later, while the oil moved initially northward, trapped at the strong density front and then spread westward along the front (Figure 4g), in agreement with the pathway of the drifters (see section 3.2.2). These findings suggest that the pathways derived from the drifters may be used to determine the hydrocarbon pathways in the topographically complicated and environmentally sensitive regions around the MR Delta region and even extending over the broader Gulf of Mexico.

All cases presented in this section are related to the northward and westward pathway of hydrocarbons along different fronts of the downstream river plume current under downwelling-favorable easterly winds.

3.2.2. Surface Currents

The speed of each drifter during characteristic periods is presented in Figure 6. The raw drifter data have spikes and drop-outs due to positioning errors and sensitivity to the orientation of the GPS antenna in the drifters, especially the undrogued ones. The spikes were removed by filtering the data with 15 min linear interpolation. Both UN2 (undrogued) and DR2 (drogued) moved northward during the first hours of their deployment on 18 April. The undrogued drifter had slightly higher speed, reaching the MR front (15 mg/m^3; Figure 6a) approximately 2 h earlier than the drogued drifter. A significant difference between the two drifters occurs during the first 12 h of their westward pathway along the front. Once trapped in the front, the undrogued drifter turned westward and its speed quickly increased up to 1.3 m/s. After reaching the front as well, the drogued drifter moved west in the same fashion and its speed increased up to 1.2 m/s 9 h later, only slightly slower than the undrogued drifter. The undrogued drifter showed higher speeds almost during the entire westward pathway. Both drifters slowed down on 21 April after they passed over the LB. Successive low and peak are observed around 20 April, before (∼0.5 m/s; Figure 6a) and after (∼1.1 m/s; Figure 6a) the anticyclonic turning of the plume bulge at 89.8°W (Figure 2a). A time lag of 4 h due to the speed difference between the two drifters is noted over this region.

The westward movement of the drifters, deployed in the morning of 20 April and presented in section 3.1, is related to the westward currents along the front (radar measurements; Figure 4e). The change in direction of the surface currents from northward (south of the front) to westward (north of the front) is apparent in the marine radar-derived current maps. The radar measurements also confirmed a respective magnitude change with weaker northward currents (∼0.3 m/s) outside the plume and stronger westward currents (∼1 m/s) inside the plume, in agreement with the UN2 and DR2 drifter trajectories and speeds (Figure 6a). The onshore shift of the front and the retreat of the river plume around the MR Delta (Figure 4) is related to these northward currents due to the southeasterly prevailing winds. It appears that similar dynamics

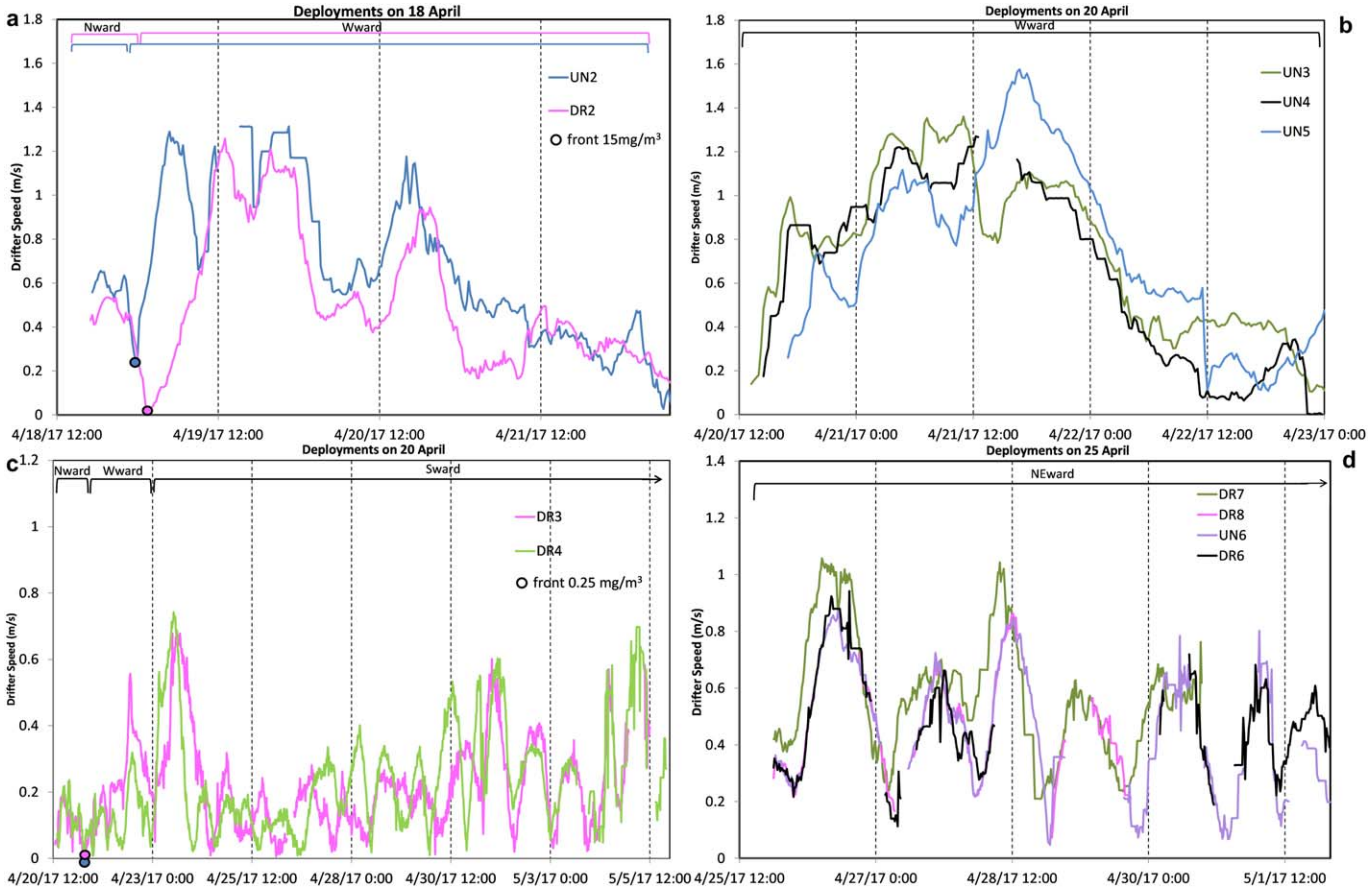

Figure 6. Propagation speed (m/s) of (a) UN2 and DR2 (deployed on 18 April), (b) UN3, UN4, and UN5 (deployed on 20 April), (c) DR3 and DR4 (deployed on 20 April), (d) DR6, DR7, DR8, and UN6 (deployed on 25 April) drifters. The colors represent the drifter trajectories presented in Figure 2. The date that a drifter reaches a plume front (0.25 or 15 mg/m^3) is marked with a circle and the major direction of the drifters' movement is also indicated at the top of each figure.

prevailed around the Taylor Energy Site on 18 April (revealed from drifters) and on 20 April (detected from radar). Drifters and radars provide complementary pieces of information on the dynamics at and around the front: the drifters show the transport pathways over several days, while the radar provides details on the velocity field around the front.

Westward spreading is also observed for the oil around the Taylor Energy Site. The darker areas in the radar images (Figure 4) show a clear oil alignment along the outer 0.25 mg/m^3 front on 20 April. The three undrogued drifters showed similar alignment during their propagation along the front, reaching a peak in their speed one day after their deployment (Figure 6b). A small lag is present for the last deployed drifter UN5 reaching the highest level of 1.6 m/s speed 7 h after the first deployed UN3 over the same area (west of 89.8°W, Figure 2b). Lower velocities ($<$0.4 m/s) occurred very close to the coast and before their coastal landings (Table 1), at the west part of the LB on 22 April.

The propagation speed of drifters DR3 and DR4 was below 0.2 m/s before their entrapment in the river front (Figure 6c), similar to the drifters released on 18 April (Figure 6a). The drifters moved northward on 20 April, in agreement with the surface oil (Figure 4), but they started to accelerate after their interaction with the stronger westward currents on 21 and especially on 22 April, reaching the level of 0.55 m/s. However, their propagation speed is significantly lower than the respective speed of the undrogued drifters (Figure 6b), which eventually reached the western coasts during the same period of time, under the effect of the surface winds (Figure 2b). The removal of the river front away from Taylor, in combination with the smaller speed of the drogued drifters and the direction change of winds that took place after 23 April, led to a completely different pathway of the drogued drifters deployed during that day. The drifter speed increased to 0.75 m/s on 23 April under westerly winds, which dragged the oiled surface waters and drifters toward the Gulf

interior. The offshore pathway of the drifters continued even when the winds changed again to southeasterly at the end of April and in early May. The drifters were dominated by the regional circulation conditions (see section 4.1). The reappearance of northwesterly winds after 4 May (Figure 3e) also enhanced the southward propagation of the drifters, increasing again their speed (Figure 6c).

The highest speeds of all drifters deployed on 25 April were detected during the first 2 days (Figure 6d) due to the strong westerly winds, which enhanced the northeastward upstream currents. The MR plume extended offshore due to the westerly winds covering the Taylor Energy Site; river waters with high chl *a* concentrations (>5 mg/m^3) were detected over the deployment area. During the deployments on 25 April, Taylor Energy Site was located approximately 25 km onshore from the outer river front (Table 1). This plume extension over Taylor was still apparent in the beginning of May (Figure 2c). The DR7 trajectory was closer to the MR Delta, along the inner front ($\sim$5 mg/m^3) in comparison to other three drifters, which propagated along the further offshore front ($\sim$2 mg/m^3). This difference resulted in 20% higher propagation speeds for DR7; speed values for most of the drifters were higher than 1 m/s on 26 April (Figure 6d). All drifters, drogued and undrogued, reduced their speed on 27 April ($\sim$0.2 m/s) when downwelling winds prevailed and inhibited the development of the upstream current. However, the drifters, entrapped along the plume fronts, kept moving toward the north. The fluctuation of the propagation speed was almost the same among all drifters, due to the similar trajectories they followed along the outer MR front. The identical behaviour of the undrogued UN6 and drogued DR8 until 2 May (Figure 2c) is also evident in the speed evolution (Figure 6d), showing that the effect of the winds (mainly affecting surface oil) and the near-surface currents (mainly affecting oil in suspension near the surface) on the hydrocarbon pathways is the same over this part of the plume region and under the specific environmental conditions.

The undrogued drifters generally revealed higher velocities and different trajectories compare to the drogued drifters. This is a strong evidence that material located directly at the surface can be transported at significantly different speed and along different pathways, from material submerged in the upper layer below the surface. Thus oil suspended in the water column could be transported quite differently from oil at the surface. The distributions of the meridian (U_x) and zonal (U_y) components of the drifter velocities are presented in Figure 7. The velocity distribution of undrogued drifters is spread over a greater range, indicating the sensitivity of this drifter type to the wind variability. Both U_x and U_y components of the undrogued drifters revealed higher values (>1 m/s; Figure 7b) than the respective drogued ones (<1 m/s; Figure 7a). In particular, the westward component of the undrogued drifters reached the levels of 1.5 m/s under strong and frequent easterly winds (68.4%; Figure 7d). The mean velocity of undrogued drifters U_x is negative (-0.015 m/s) indicating prevailing westward velocities in agreement with the negative zonal wind (W_x) component (–0.008; Figure 7c), while the respective velocity of drogued drifters is positive (0.028 m/s, eastward). The large (UN $>$ 0.5 m/s, Figure 7d) westward velocities of the undrogued drifters revealed significantly higher occurrence frequency (6.0%), in comparison with all other directions of both types, although the northward wind component was the highest (74.3% for all magnitudes and 17.2% for strong winds). The existence of the river front north of and very close to the drifter deployment site in most cases was able to reduce the northward propagation of the drifters and enhance the westward transport. Fewer southward velocities (negative values) are observed for the undrogued drifters due to the low frequency of northerly (25.7%) and westerly (31.6%) winds during the field experiment. The southward entrainment is stronger in the drogued case (55.9%), due to both wind effect and regional circulation (see section 4.1). The mean drogued U_y is negative (–0.015; Figure 7a), indicating prevailing southward velocities, while the respective undrogued is positive (northward; Figure 7b). The drogued drifters reveal an equivalent distribution with smaller range of frequencies for the velocities larger than 0.5 m/s (1.5%–2.0%), in comparison to the respective undrogued drifter range (1.3%–6.0%).

4. Discussion

4.1. Regional Circulation Effects on Oil Pathways

Several major circulation patterns over the NGoM and specifically the MR plume pathways are strongly determined by regional circulation, such as the formation of local eddies (Androulidakis & Kourafalou, 2013; Schiller et al., 2011; Walker et al., 2005) and the general evolution of the LC system (Le Hénaff & Kourafalou, 2016; Schiller & Kourafalou, 2014; Walker et al., 2011). The LC evolution and the shedding events of the LCE may take place very close to the northern continental shelves and the broader MR Delta region (Zavala-

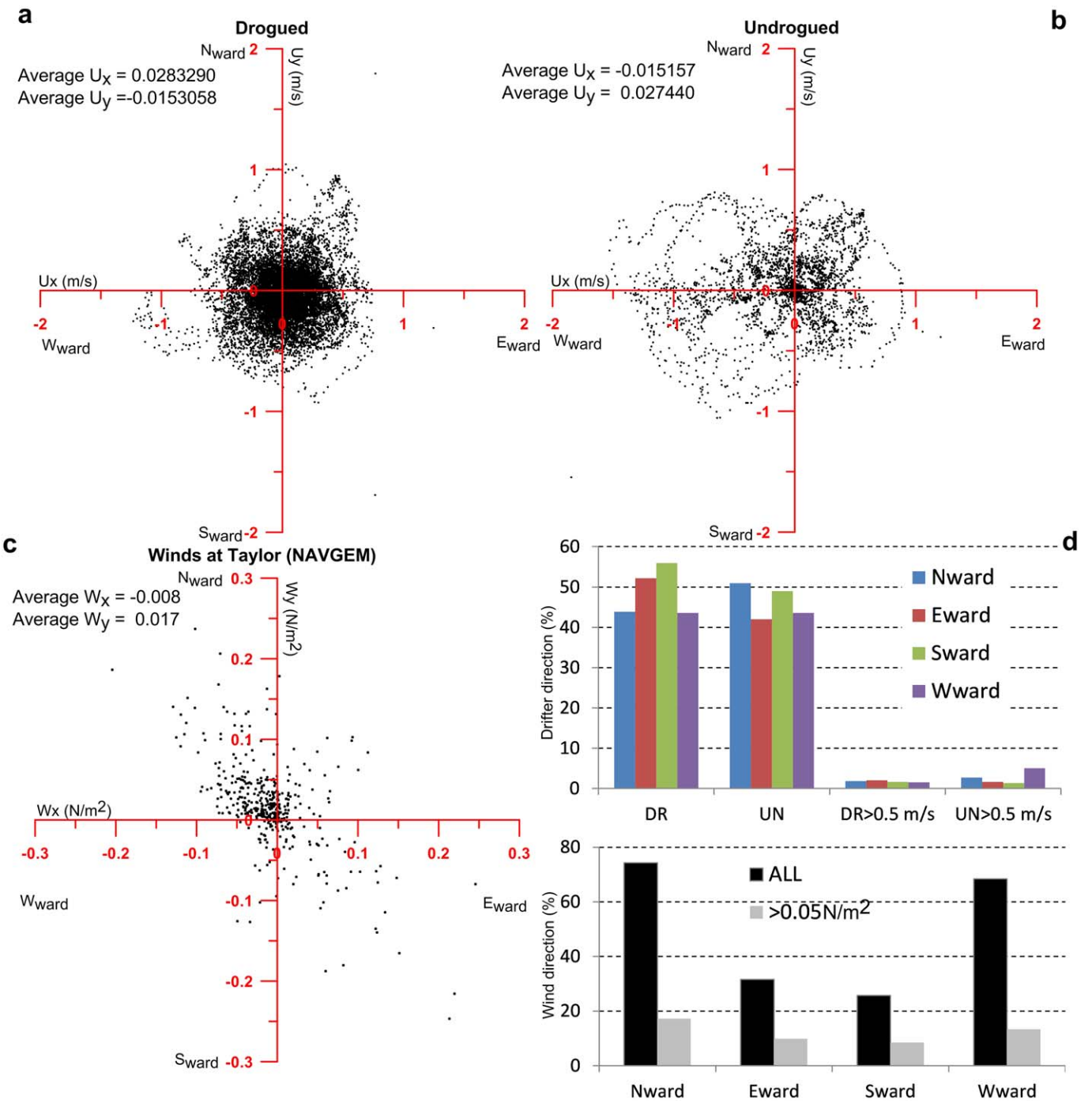

Figure 7. Scatter diagrams of velocity vector components (U_x and U_y; m/s) derived from all (a) drogued (DR) and (b) undrogued (UN) drifters. (c) Scatter diagram of wind stress vectors (W_x and W_y; N/m^2) derived from the Navy Global Environmental Model (NAVGEM) fields at Taylor Energy Site during the drifter experiment (April–June 2017). (d) Occurrence frequencies for both types and each propagation direction (Northward: N_{ward}, Eastward: E_{ward}, Southward: S_{ward}, and Westward: W_{ward}) for the wind stress vectors are presented in two bar diagrams (for all velocities and wind stresses and for the values that exceed 0.5 m/s and 0.05 N/m^2, respectively). The U_x, U_y, W_x, and W_y means are also shown.

Hidalgo et al., 2006). The offshore propagation of the drogued drifters deployed on 20 April is presented in Figure 2b, when a narrow offshore patch of high chl *a* waters is also evident along the southward track of the drifters. We showed that the initial southward propagation of the drifters between 23 April and 26 April was related to the domination of northwesterly winds over the region. The second period with strong

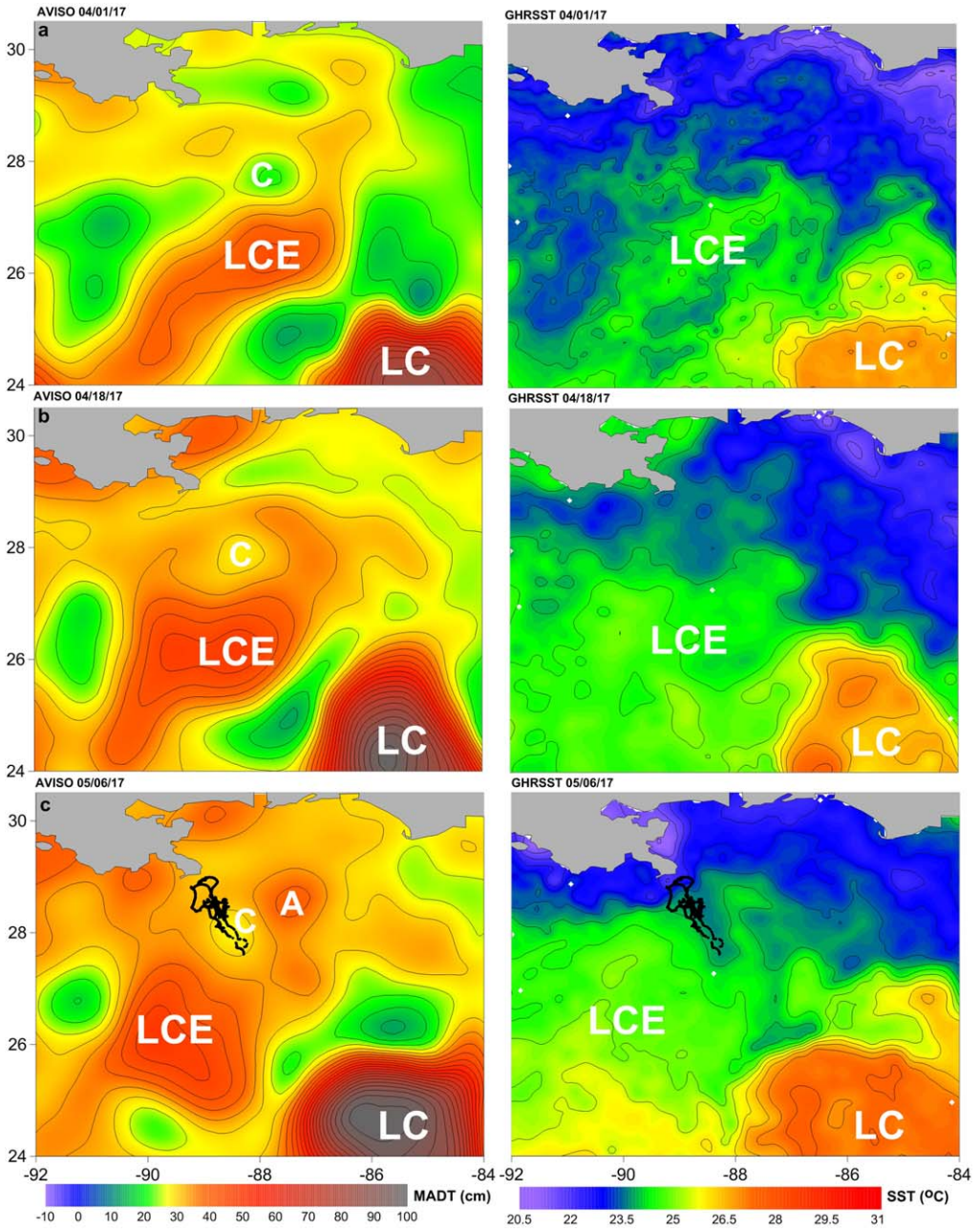

Figure 8. (left) Maps of Absolute Dynamic Topography (MADT; cm) derived from the Archiving, Validation and Interpretation of Satellite Oceanographic (AVISO) database on (a) 1 April, (b) 20 April, and (c) 6 May. (right) The respective maps of Sea-Surface Temperature (SST; °C) derived from the Group for High Resolution Sea Surface Temperature (GHRSST) database on 06 May are presented. The Loop Current (LC), LC Eddy (LCE), and the pathways of the three drogued drifters, deployed on 20 April, until 6 May are also shown. The anticyclonic eddy (A) detached from the main LCE under the effect of a cyclonic eddy (C) is also marked.

westerly winds that may favour the formation of the southward extension of the MR plume is detected between 4 May and 7 May. Although the period in between (27 April to 3 May) is characterized by south-easterly winds, which tend to enhance the northward currents and even fully block the southward flows, both drifters and ocean color data support an opposite southward pathway toward the Gulf interior. This suggests influence of oceanic flows, which are dominated by the LC system.

The main LC body and the anticyclonic LCE evolved over the central and northern parts of the Gulf (high MADT levels), respectively, during April (Figure 8a). The LC main body was located over the central Gulf,

while two cyclonic LCFEs (low MADT levels) were located between the LC and the detached LCE, approximately at 25°N and 26°N approximately on 1 April (Figure 8a). Higher SSTs were detected over the LC region, while the NGoM was covered by colder waters (<23.5°C). Seventeen days later, the LCE remained detached from the LC and more extended over the central Gulf, although it was still away from the NGoM (<27°N; Figure 8b). A large LCFE kept the LCE and the LC separated, although the LC revealed a clear northward extension north of 26°N. This northward extension and the simultaneous LCFE weakening north of the LC played a role on the westward shift and enlargement of the LCE on 18 April. Warmer water masses are observed over the central and northern areas, closer to the MR Delta. The enlargement of the LCE increased the SST over the entire region below 28°N (~25°C). A clear westward shift and a south to north spreading of the LCE is presented in the MADT map on 6 May (Figure 8c). A secondary anticyclonic eddy ("A," Figure 8c) was detached from the main LCE at 87.5°W, around 28°N, under the influence of a small cyclonic eddy ("C") initially located at 88°W, 28°N on 1 April (patch of low MADT, Figure 8a). The clockwise circulation of the main LCE, together with the counterclockwise circulation of the small cyclonic eddy C created a dipole favouring an offshore jet south of the MR Delta. This is a process that has been documented to create strong and narrow offshore pathways in this region (Schiller et al., 2011; Schiller & Kourafalou, 2014). The result brought the drifters close to each other and moving offshore (Figure 8c), over the plume waters with slightly higher chl *a* presented in Figure 2b. The northern part of the LCE was extended along this pathway, reaching the shelf west of the MR Delta (south of the LB). This narrow offshore plume is also detected in the SST spatial distribution, where a tongue of lower surface temperature waters (~23.5°C) is observed along the merging drifter pathways, reaching an area south of 28°N by 6 May (Figure 8c), while the rest of this area is covered by warmer waters (~25°C). Higher SSTs were detected at a higher latitude (>28°N) due to the LCE northern extension. The propagation of the three drogued drifters together with some MR waters toward the central Gulf prevailed against the dominant winds that were mainly easterlies over this offshore region, which were favoring the westward and northward pathways. However, wind-driven currents had an indirect effect by narrowing the offshore MR patch, as they directed currents toward the LCE, where they were deviated offshore. The narrowness of the patch was marked by an offshore jet that kept the drifters very close along their southward pathway (Figure 8c).

4.2. Vertical Structure of the Upper Ocean

Our results suggest that the location of the plume's multiple fronts, which is determined by buoyancy and wind-driven currents in combination with regional circulation, played a significant role in the formation of different potential pathways of the hydrocarbons found around the Taylor Energy Site. The location of river fronts is also related to the vertical structure of the upper ocean over Taylor. We examine the characteristics of the ocean stratification, as they are very important in regions with thousands of oil rigs like the NGoM, where the hydrocarbons can be even released from the bottom of the sea (e.g., DwH accident in 2010). The water column structure, especially the existence of strong pycnoclines, may play a significant role on the oil rising and, therefore, on the quantity and characteristics of the oil that may finally reach the surface (Fabregat Tomàs et al., 2016; Socolofsky et al., 2011)

The density distribution along the two sections S1 and S2, collected by the Acrobat instrument aboard the R/V Walton Smith in the morning of 20 April (Figure 9), agrees with the plume signature derived from the TSG surface measurements (Figure 5) and ocean color images (Figure 4 and Table 1). The surface density, mainly controlled by salinity, decreased below 1,024 kg/m^3 at a short distance (~700 m) to the north of the Taylor Energy Site. We showed that this strong density front blocked the northward propagation of the oiled waters toward the Delta. The surface levels (2–3 m) are below 1,020 kg/m^3, while the deeper values down to 7 m depth are between 1,023 and 1,024 kg/m^3. The river plume is slightly deeper down to 10 m in the northern area of the outer river front, while very low values (1,018–1,019 kg/m^3) were measured inside the upper 5 m. Values greater than 1,024 kg/m^3 were detected in the entire water column below 10 m, with even denser water masses below 40 m. The density front location is also confirmed by the ocean color chl *a* surface concentrations in the morning of 20 April (insert in Figure 9). The clearer ocean waters with very low chl *a* concentrations (<0.25 mg/m^3) south of the front are characterized by higher density levels along the entire column of the upper ocean (>1,025 kg/m^3). The onshore shift of the front removed the low salinity waters further away from Taylor later that day (section 3.2.1).

Similarly, the CTD measurements (Figure 10a) agree with the Acrobat profile over the Taylor Energy Site. Surface density derived from the CTD measurements is around 1,024.8 kg/m^3, while both Acrobat sections

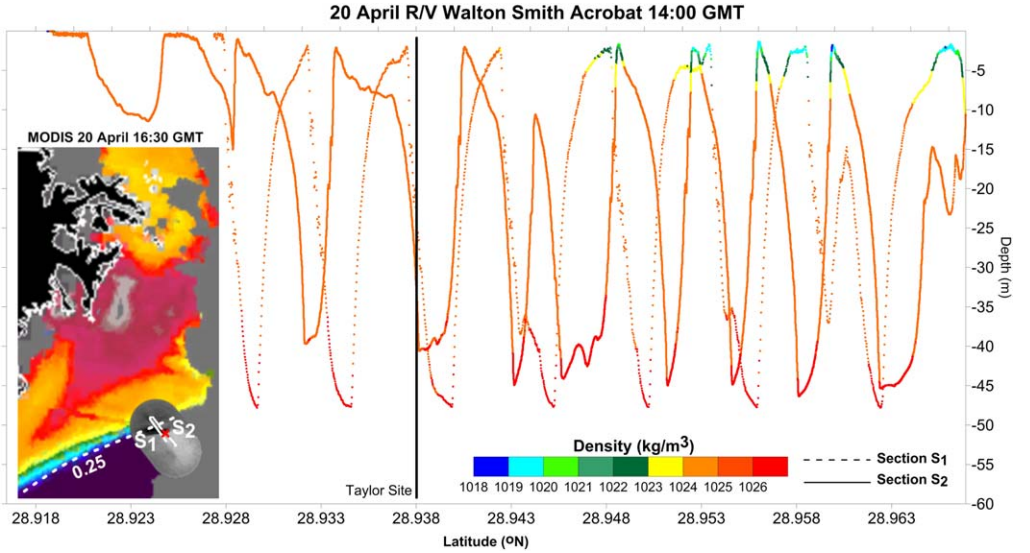

Figure 9. Density profiles along sections S_1 (dashed) and S_2 (solid) derived from the R/V Walton Smith Acrobat measurements on 20 April 14:00 GMT. Sections S_1 and S_2 are marked on the ocean color image (20 April 16:30 GMT) derived from MODIS (insert). The respective marine radar image over the area is also shown. The vertical solid black line (Acrobat plot) and the red cross symbol (insert) indicate the location of the Taylor Energy Site. The white dashed line indicates the 0.25 mg/m^3 contour of chl *a* concentration. In the ocean color image, black represents land, dark grey represents clouds or other image artifacts, while light grey, dark red, and orange represent high chl *a* concentrations.

show values near 1025 kg/m^3 around the oil source (solid black line in Figure 9). Moreover, the upper ocean down to 40 m is well mixed according to the density profiles derived from both CTD and Acrobat observations. Because the Taylor Energy Site was in the vicinity, but outside (south) the river plume in the morning of 20 April, the upper ocean at that site was observed to be homogenous with the density distribution below the mixed layer mainly controlled by temperature (Figure 10), in contrast to the area north of the front controlled by salinity (Figures 5 and 9). The salinity change in vertical is small (~0.2). Temperature significantly decreased from 40 m to 110 m (~3.5°C), leading to a respective density increase (~1.5 kg/m^3). The computed Brunt-Väisälä frequency (N^2; Figure 10b), a stratification parameter, shows very low values

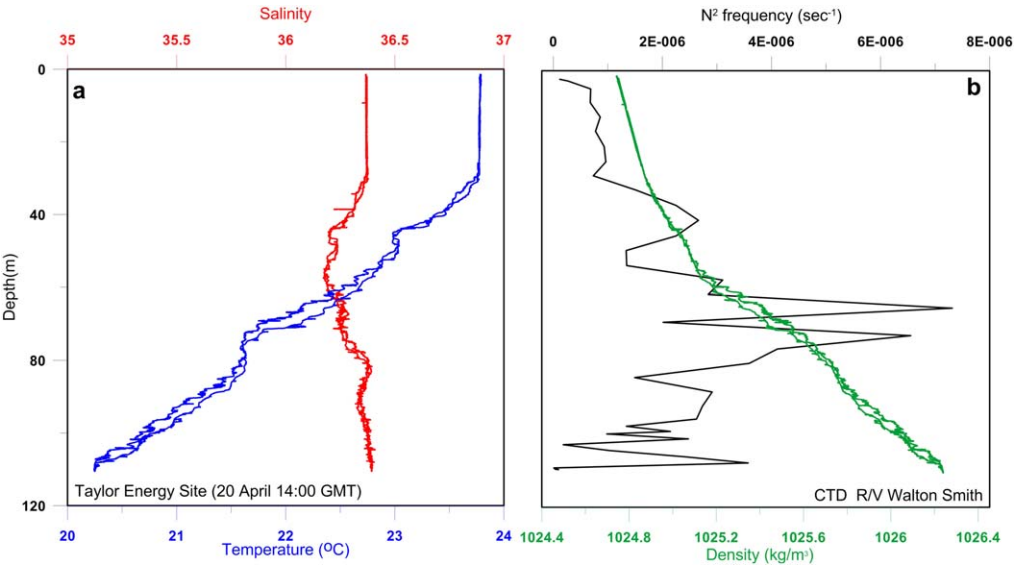

Figure 10. (a) Vertical distribution of salinity (red) and temperature (blue; °C) measured by the R/V Walton Smith CTD over the upper 110 m at the Taylor Energy Site on 20 April 14:00 GMT. (b) Vertical distribution of density (green; kg/m^3) and Brunt-Väisälä frequency (black; N^2; s^{-1}) derived from the CTD measurements.

over the upper 40 m and a more stratified ocean in deeper layers with significantly higher values around 70 m, where strong temperature decrease occurs. No pycnocline was observed at Taylor on 20 April, while the upper ocean (down to ~110 m) was generally stratified below 40 m with a homogenous water mass over the upper layers. This was not the case on 18 April, when the river plume was more offshore and extended over Taylor, forming a potential barrier with low salinity layer in the upper 10 m, as presented in Figure 9. This barrier may delay and/or reduce the hydrocarbons from reaching the ocean surface in the case of a bottom leakage anywhere near NGoM, within river plume influence. Further investigation (out of the scope of the present study) is needed to determine the effects of ocean structure on the hydrocarbon propagation from bottom to surface. The depth of the plume (5–10 m) detected in the Acrobat measurements ensures our assumption (section 2.1) that the drogued drifters were generally under the influence of the brackish plume and its associated dynamics. These drifters, that followed subsurface currents (~1 m), were trapped and propagated along the river fronts.

4.3. Oil Spreading Patterns During the Field Experiment

The northward short spreading of the oil under southeasterly winds (Figure 3b) on 20 April is evident in the marine radar images (Figure 4). The onshore shift of the river front during the day removed the brackish plume away from the Taylor Energy Site. The northward currents spread the hydrocarbons toward the front, where they were trapped and finally propagated westward, along the downstream plume current. We also employ satellite imagery (section 2.3) to characterize frontal displacements. The oil pattern observed in the shipborne radar was also captured by the RADARSAT-2 SAR image (dark pixels in Figure 11a). A clear cone-shape oil patch (~3 km at its widest part) spread from Taylor up to the front. The clear ocean waters cover the area around the cone and south of the river front. The MR plume was located north of the density front, while a thin strip of oil was aligned along the front and moved westward. No oil was observed north of the front or inside the plume, in either marine radar or SAR images, in agreement with findings by Kourafalou and Androulidakis (2013), who showed that the river plume was able to block the DwH oil spill from approaching the Delta in mid-June 2010, when its upstream (northward) pathway dominated. The UAS aerial image confirms the northward spreading of the surface oil and its entrapment along the front (Figure 11b). The east-west alignment of the river front and the south-north strips of oil between the Taylor Energy Site and the river front are both apparent in the drone imagery, while no oil is observed north of the front.

The offshore pathway derived from the drogued drifters on 25 April is also confirmed with the oil spreading captured by high-resolution imagery from three different satellites (Figure 12). The half-moon shape of oil around Taylor due to the effect of the westerly winds is similar to the trajectories of drifters DR4 and DR5 that were deployed at 2 h interval on 20 April and started to move offshore on 23 April (Figure 12a), when the wind direction changed from easterly to westerly (Figure 3b). The 15 m resolution Aster image (Figure 12b) shows both the position of the river plume (light blue) and a distinctive thick oil pattern (white half-moon shape). Thinner patches of oil (pink) are detected in the east side of the thicker oil due to the prevailing westerly winds that may spread the surface waters, containing thin oil toward the east. Although patches of thin oil are also detected southwest of the thicker oil, that area is very limited in comparison to the thin oil observed at the east side of the thicker oil. The drogued drifters, affected mainly by subsurface currents, moved southeastward along a trajectory similar to the shape of the thick oil patches. This is an indication that near-surface drifter trajectories can be representative of surface movement of thick oil slicks under such environmental conditions. The thick oil patches are also evident in the 1.5 m resolution WorldView-2 image (Figure 12c) confirming the southward spreading, in agreement with the drogued drifter pathways. It is noted that the WorldView-2 image includes only the northern part of the thick oil patch presented in the other two satellite images. The river plume is located north of the Taylor Energy Site; the dark grey parts of the plume are characterized by less suspended material, while the inner (northwestern) part of the plume is covered with large quantities of suspended matter (light grey). Areas with more suspended material are characterized by higher reflectiveness and thus lighter color in the satellite image.

The four drifters deployed on 25 April at the Taylor Energy Site described the northeastward spreading of the oil, captured by the 18 m resolution TerraSAR-X SAR image on 26 April (Figure 13a). The red area is an oil delineation obtained by the Textural Classifier Neural Network Algorithm (Garcia-Pineda et al., 2009). The northeastward movement of the oil is similar to the drifter tracks; on 26 April the drifters were located very

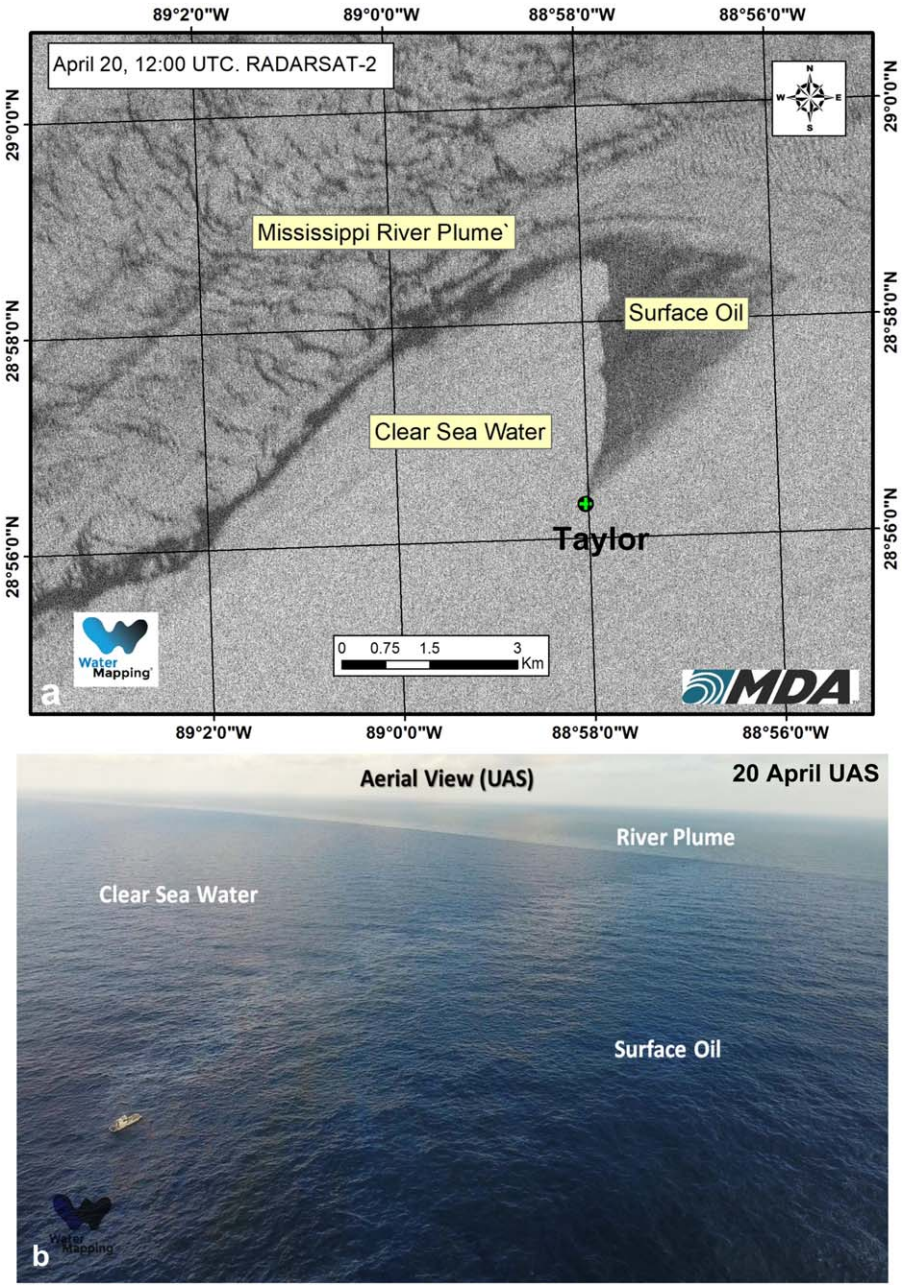

Figure 11. Images collected from (a) RADARSAT-2 satellite and (b) Unmanned Aerial System (UAS) aerial view on 20 April. The Mississippi River plume, the Taylor Energy Site, the clear sea water and the surface oil are marked. The R/V St. Anthony (13 m) is shown in the UAS image. RADARSAT-2 Data and Products © MDA (2017) – All Rights Reserved.

close to the eastern part of the oil patch shown in the satellite image (<1 km). The total length of the oil patch visible to the satellite was around 6 km with 1 km mean width. The prevailing westerly winds determined the undrogued UN6 trajectory while the subsurface currents carried drogued DR6, DR7, DR8 drifters along the front of the upstream current. Therefore, it is possible that both surface oil and subsurface suspended oil might followed this pathway and were carried away by the upstream current, toward the MAFLA shelf. The DR7 was located closer to the oil (∼500 m) and propagated further to the north, in comparison with the other three drifters, during the first hours after the deployment. The influence of wind change from northwesterlies to southeasterlies after 27 April was also captured in the oil spreading on 28 April (Figure 13b). The downwelling-favorable winds blocked the evolution of the upstream current close to

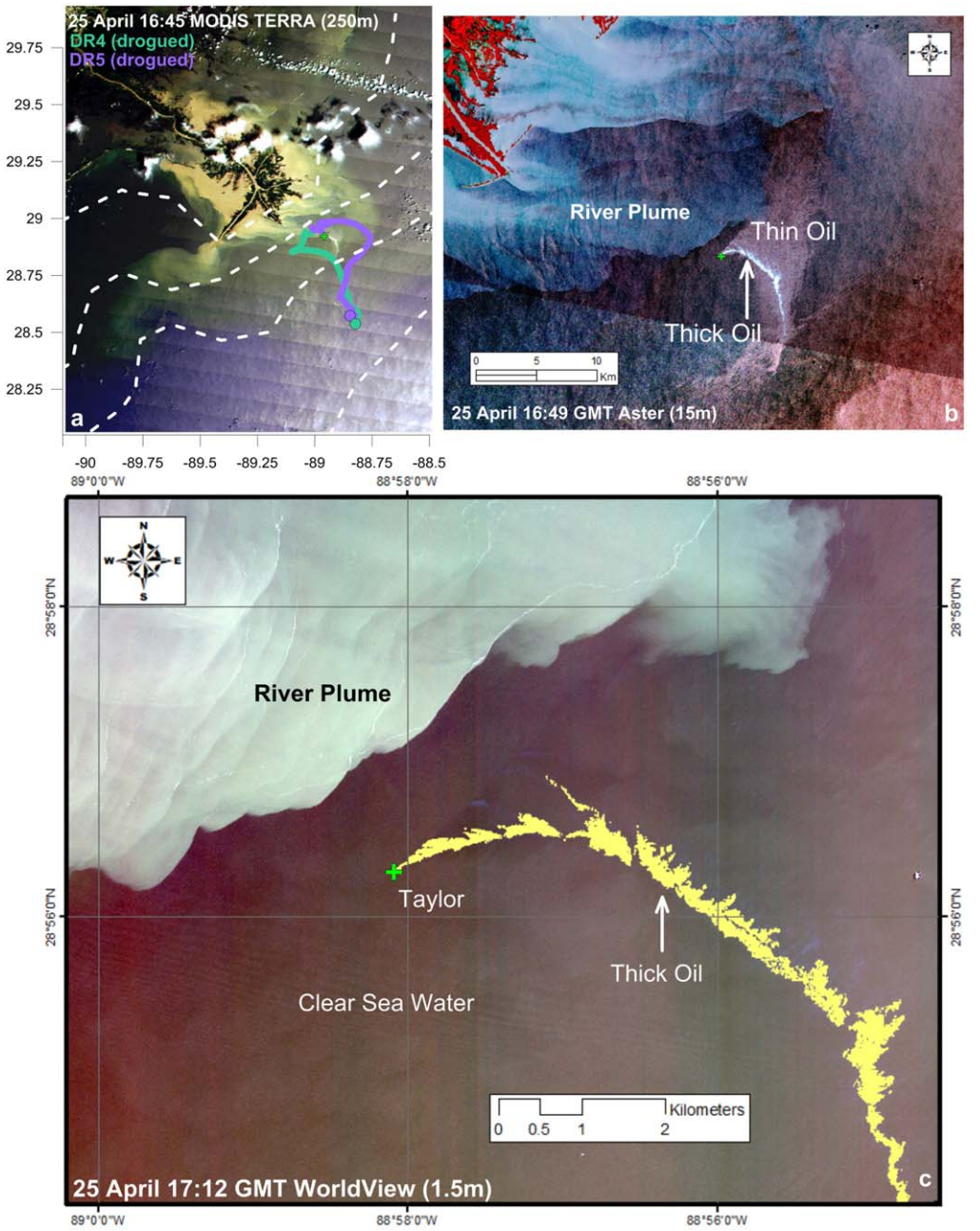

Figure 12. Images collected from (a) MODIS TERRA (250 m resolution), (b) Aster (15 m resolution) and WorldView-2 (1.5 m resolution) satellites on 25 April. The trajectories of drifters DR4 (green) and DR5 (purple) from their deployment on 20 April until 25 April are presented in Figure 12a. The Mississippi River plume (blue shade in b and white shade in c), the clear sea water, the Taylor Energy Site (green cross) and the thick surface oil (white in Figures 12a and 12b and yellow in Figure 12c) and the thin surface oil (pink patch in Figure 12b) are also marked.

Taylor and, consequently, the spreading of surface waters and oil toward the MAFLA shelf. The northeastward spreading was limited, destroying the clear and straight cone-shape oil patch, although its size and length was tripled. However, the initial dominance of westerly winds in early May, in combination with the increasing MR discharge during May, enhanced the upstream plume evolution along the MAFLA shelf, carrying the drifters toward the east (section 3.1). It is noted that the oil patches over the Taylor Energy Site are strongly influenced by the prevailing wind conditions.

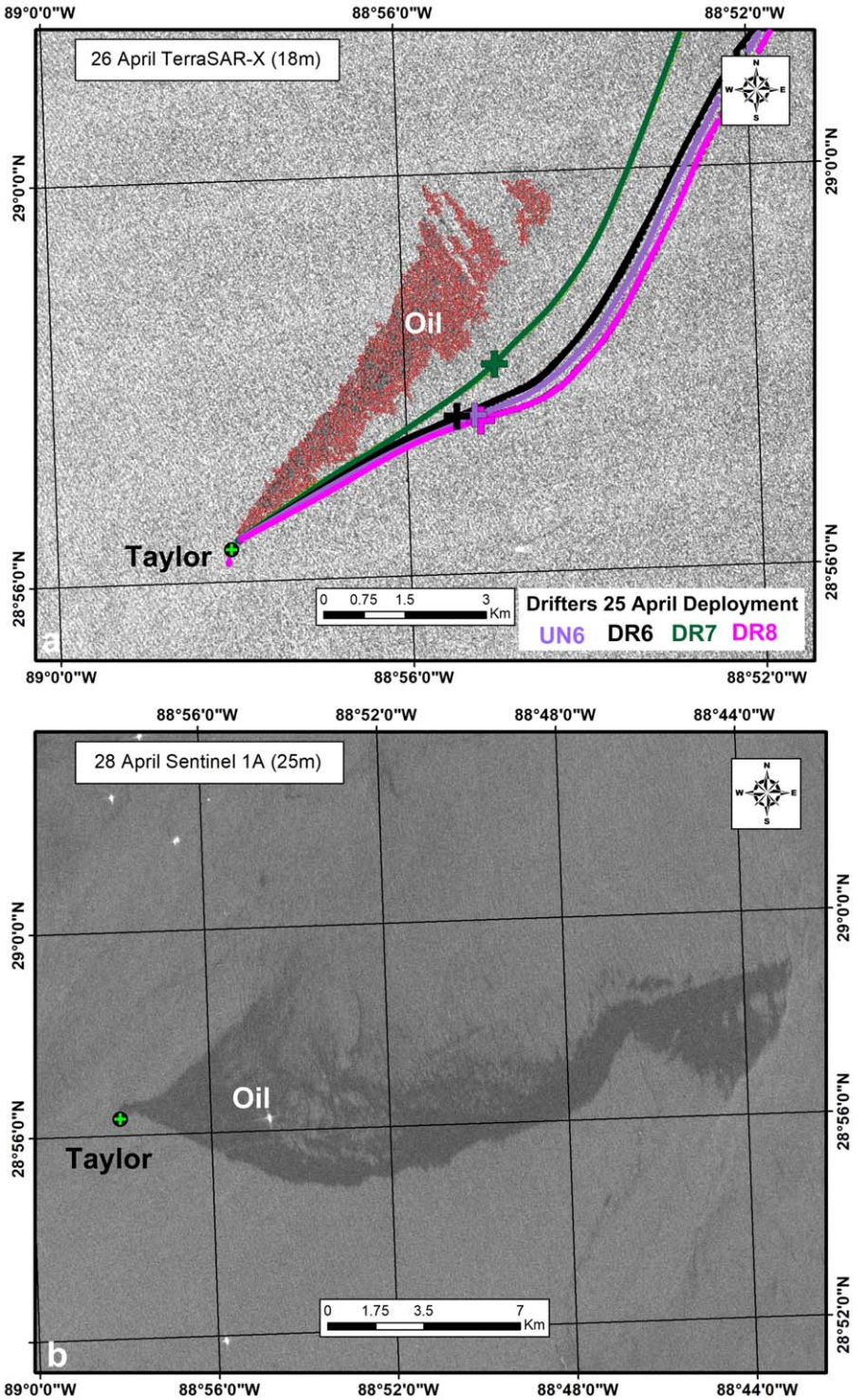

Figure 13. Images collected from (a) TerraSar-X (18 m resolution) and (b) Sentinel-1 (25 m resolution) satellites on 26 and 28 April, respectively. The trajectories of UN6, DR6, DR7, and DR8 drifters deployed at Taylor Energy Site (indicated with a green cross marker) on 25 April are also shown on top of the TerraSar-X image. Crosses indicate the location of the drifters on 26 April 00:00 GMT. TerraSAR-X data © 2017 DLR e.V., Distribution Airbus DS.

5. Conclusions

Our results demonstrate that oil may be trapped along the fronts induced by the Mississippi River (MR) plume. The development of fronts due to the strong density differences between the brackish water masses and the clearer high salinity ocean blocked the onshore propagation of both drifters and oil toward the MR Delta. It is shown that atmospheric and oceanic processes (specifically wind and regional circulation) played a significant role in the evolution of the fronts and in the formation of different potential pathways of the hydrocarbons found around the Taylor Energy Site. We conclude that the location of riverine fronts, the proximity of oil slicks and the prevailing winds are important inter-dependent factors triggering initial pathways that determine the fate of hydrocarbons potentially released near the Mississippi Delta, toward the NGoM coastlines or over the broader Gulf of Mexico (GoM). We found that the understanding of such pathways requires the documentation of MR plume pathways and the understanding of the related dynamics. We found transport pathways extending to the east and west of the MR Delta, following major current regimes influenced by this major river plume. Some of the drifters landed either on Louisiana-Texas (LATEX) or Mississippi-Alabama-Florida (MAFLA) coasts, suggesting that hydrocarbons released around the Taylor Energy Site and close to the MR Delta have the potential to reach several coastal Northern GoM (NGoM) locations. It is noted that the magnitude of such potential effects largely depends on the quantity of the oil and the dimensions of a certain spill, which are vital factors on the final destination and impacts of the related hydrocarbons. The pathways derived from the drifter trajectories were corroborated by the distribution of surface currents and the oil spreading at the Taylor Energy Site and along the river fronts, derived from marine radar and high-resolution satellite data. These results suggest that the drifter observations can be used to determine surface and near-surface hydrocarbon pathways at topographically complicated and environmentally sensitive regions such as around the MR Delta and the broader GoM. The different types of drifters showed a diverse behaviour under specific environmental conditions. It is possible that drogued/undrogued drifters could be used in future experiments to trace thin/suspended oil patches, assuming that these are primarily affected by surface/subsurface currents. However, a more careful investigation about the relation between the oil thickness and the final oil pathways is needed and is part of an ongoing study.

All main pathways derived from our multiplatform observational study are presented in Figure 14. The drifter trajectories, deployed on 18, 20, and 25 April 2017, described all the major circulation patterns over the broader NGoM region around the MR Delta (Figure 14a). These patterns are strongly related to the potential hydrocarbon pathways of the oil found around the Taylor Energy Site (Figure 14b). The first pathway, westward along the downstream river plume current, is more dominant and is able to transfer hydrocarbons over the LATEX continental shelf. This pathway was basically formed under the effect of the downwelling-favorable easterly winds that prevailed during the experiment. Undrogued drifters had higher speeds (mean velocity: $V_{UN} = 0.63$ m/s) along the downstream pathway, indicating the possibility that surface oil can spread faster toward the west in comparison with subsurface oil in suspension (drogued drifters, $V_{DR} = 0.33$ m/s) and generally with hydrocarbons that may be transported either offshore (southward; $V_{DR} = 0.22$ m/s) or over the MAFLA shelf (upstream; $V_{UN} = 0.45$ m/s and $V_{DR} = 0.44$ m/s). The coastal landing west of the Louisiana Bight (LB) is strongly related to the onshore shift of the downstream front closer to the coast over this area that can potentially allow hydrocarbons to reach land under downwelling-favorable wind conditions. No coastal landing was observed along the LB coast.

The second major pathway is described by the drifters that propagated northeastward along the MAFLA shelf, along the upstream river plume front. This pathway was formed due to the effect of strong westerly winds that prevailed during the drifter deployments on 25 April, driving surface waters along the fronts induced by the upstream MR plume propagation. The initial movement of the drifters along either onshore or offshore fronts determined their final pathway and the possibility of coastal landing on the MAFLA coast. The upstream pathway along fronts closer to the shore was faster, probably due to the stronger currents over the inner parts of the plume along its upstream propagation. The strong river discharge rates of May 2017, in tandem with a second period of westerly winds in early May, contributed to the accumulation of large quantities of riverine waters over the MAFLA shelf, enhancing the upstream currents and maintaining the eastward pathway along the northern coasts for both drogued and undrogued drifters.

The third pathway, derived from this multiplatform observational study, is the southward offshore transport toward the Gulf interior. Both wind and regional circulation effects contribute to the evolution of this

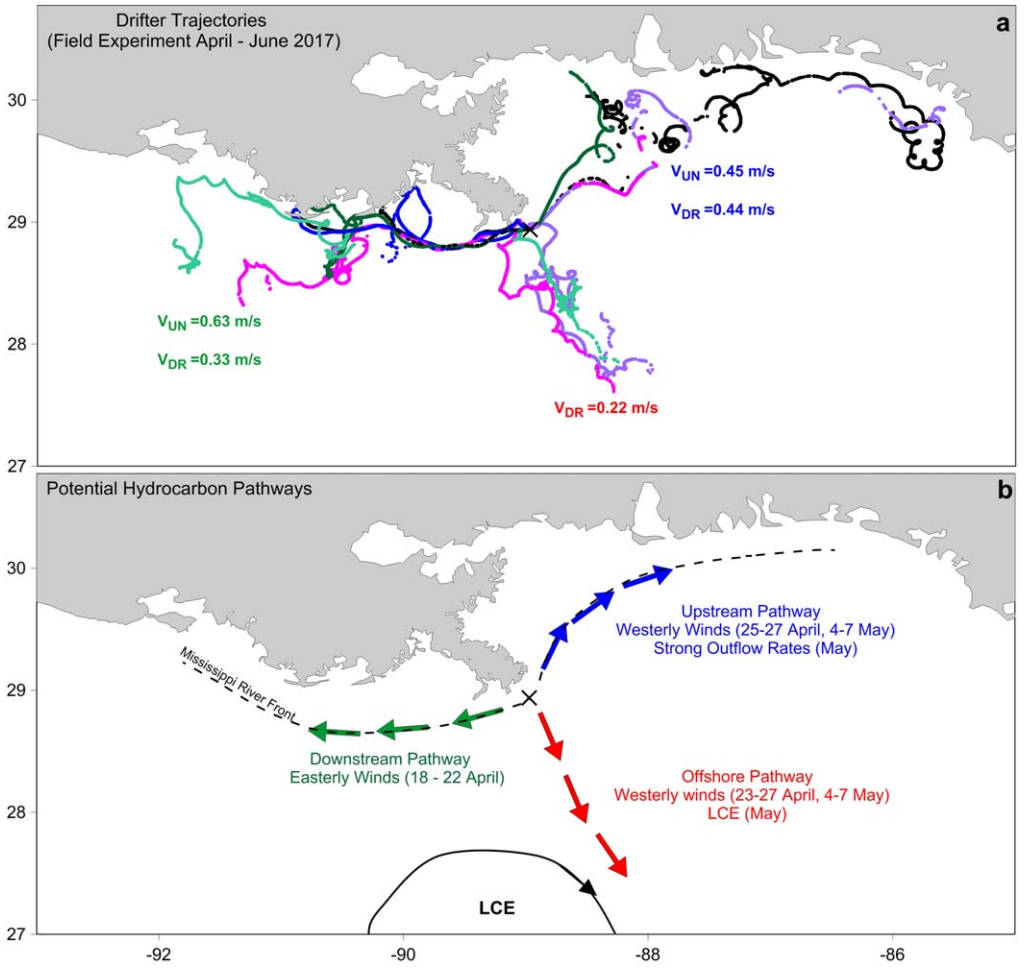

Figure 14. (a) Overall drifter trajectories derived from the April–June experiment (for trajectory colors see Table 1) and (b) characteristic periods showing the three potential hydrocarbon pathways (downstream: green; upstream: blue; offshore: red), the Mississippi River front and the Loop Current Eddy (LCE) pattern during the April–June 2017 field experiment (indicated by color arrows, dashed line and solid line with a black arrow, respectively). The mean drogued (V_{DR}) and undrogued (V_{UN}) velocities and the prevailing wind directions for each pathway are also marked.

pathway that may transfer oil, originating over NGoM and around the Taylor Energy Site, to remote Gulf areas. The Loop Current (LC) Eddy (LCE) evolution over the region, in tandem with easterly winds, kept the slower drogued drifters (that were deployed at the Taylor Energy Site on 20 April) very close to each other and led them along a narrow branch of low salinity toward the south. This pathway was strongly influenced by the general LC system and it indicates that a potential future large oil spill in this area may lead hydrocarbons to remote southern Gulf regions and through the Straits of Florida toward the Atlantic Ocean, similar to patterns of MR plume waters that have been documented in several studies.

The evolution of river fronts over the Taylor Energy Site and along the downstream and upstream pathways affected the drifter trajectories and final destination, trapping both drifters and oil patches along the fronts. During the field study period, the Taylor Energy Site was located either inside the plume waters (e.g., 18 April) or south of the outer river front (e.g., 20 April). This variability had a profound influence on the advection of oiled waters. The onshore-offshore shift of the front over the Taylor Energy Site may result to different drifter pathways and oil spreading, as they are first trapped along the plume and then propagate under the influence of the prevailing wind conditions over the area. In situ thermohaline measurements around the Taylor Energy Site and across the river fronts showed that the MR plume, characterized by low salinity values, was 5–10 m deep near Taylor, while a homogenous clear ocean layer of 40 m was detected outside the plume. The existence of strong pycnoclines due to river plumes, besides the effects on the horizontal

transport of the oil, can play a significant role on the rise of oil toward the surface and the fate of hydrocarbons in the case of bottom leaks (as was the case of the 2010 Deepwater Horizon accident). The ocean vertical structure, in combination with the determination of the source of the hydrocarbons that were observed in the surface of the Taylor Energy Site, is a very important topic and requires further investigation.

Acknowledgments
This research was made possible by two grants from The Gulf of Mexico Research Initiative (award "Influence of river induced fronts on hydrocarbon transport," GOMA 23160700 and award "Consortium for Advanced Research on Transport of Hydrocarbon in the Environment," CARTHE). M. Le Hénaff acknowledges partial support from the Physical Oceanography Division at NOAA's Atlantic Oceanographic and Meteorological Laboratory, AOML. The high-resolution ocean chl *a* images were produced by the Optical Oceanography Laboratory (University of South Florida; http://optics.marine.usf.edu). The mapped altimetry (AVISO) products were produced by the Ssalto/Duacs multimission system and distributed by the Copernicus Marine and Environment Monitoring Service (CMEMS; http://www.marine.copernicus.eu). The MUR Global High-Resolution SST data set was distributed by NASA (http://podaac.jpl.nasa.gov/dataset/JPL-L4UHfnd-GLOB-MUR). The wind time series for the Taylor Energy Site was derived from the Navy Global Environmental Model (NAVGEM; https://hycom.org/dataserver/navgem). We acknowledge the kind support from Davida Street and Ellen Ramirez from the Satellite Analysis Branch (NOAA NESDIS), and the invaluable help from Gordon Staples MDA Corporation. Two MetOcean drifters were provided through the RETROSPECT project sponsored by the Research Council of Norway (RCN grant 244262) and led by Kai Christensen of the Norwegian Meteorological Institute. The drifter data, the observations collected from R/V Walton Smith, and the satellite data are available through The Gulf of Mexico Research Initiative Information and Data Cooperative (https://doi.org/10.7266/N7GH9GC2, https://doi.org/10.7266/N75719MJ, https://doi.org/10.7266/N74J0CKB, https://doi.org/10.7266/N7RR1WV5, and https://doi.org/10.7266/N7V69H4N; https://data.gulfresearchinitiative.org/). We thank the two anonymous reviewers for their constructive comments.

References

Androulidakis, Y. S., & Kourafalou, V. H. (2013). On the processes that influence the transport and fate of Mississippi waters under flooding outflow conditions. *Ocean Dynamics*, *63*(2–3), 143–164.

Androulidakis, Y. S., Kourafalou, V. H., & Schiller, R. V. (2015). Process studies on the evolution of the Mississippi River plume: Impact of topography, wind and discharge conditions. *Continental Shelf Research*, *107*, 33–49.

Berta, M., Griffa, A., Magaldi, M. G., Özgökmen, T. M., Poje, A. C., Haza, A. C., et al. (2015). Improved surface velocity and trajectory estimates in the Gulf of Mexico from blended satellite altimetry and drifter data. *Journal of Atmospheric and Oceanic Technology*, *32*(10), 1880–1901.

Braun, N., Ziemer, F., Bezuglov, A., Cysewski, M., & Schymura, G. (2008). Sea-surface current features observed by Doppler radar. *IEEE Transactions on Geoscience and Remote Sensing*, *46*(4), 1125–1133.

Crone, T. J., & Tolstoy, M. (2010). Magnitude of the 2010 Gulf of Mexico oil leak. *Science*, *330*(6004), 634.

Davis, R. E. (1985). Drifter observations of coastal surface currents during CODE: The statistical and dynamical views. *Journal of Geophysical Research*, *90*(C3), 4756–4772.

Donlon, C. J., Casey, K. S., Robinson, I. S., Gentemann, C. L., Reynolds, R. W., Barton, I., et al. (2009). The GODAE high-resolution sea surface temperature pilot project. *Oceanography*, *22*(3), 34–45.

Fabregat Tomàs, A., Poje, A. C., Özgökmen, T. M., & Dewar, W. K. (2016). Dynamics of multiphase turbulent plumes with hybrid buoyancy sources in stratified environments. *Physics of Fluids*, *28*(9), 095109.

Falcini, F., Khan, N. S., Macelloni, L., Horton, B. P., Lutken, C. B., McKee, K. L., et al. (2012). Linking the historic 2011 Mississippi River flood to coastal wetland sedimentation. *Nature Geoscience*, *5*(11), 803.

Garcia-Pineda, O., MacDonald, I., Hu, C., Svejkovsky, J., Hess, M., Dukhovskoy, D., et al. (2013). Detection of floating oil anomalies from the Deepwater Horizon oil spill with synthetic aperture radar. *Oceanography*, *26*(2), 124–137.

Garcia-Pineda, O., Zimmer, B., Howard, M., Pichel, W., Li, X., & MacDonald, I. R. (2009). Using SAR images to delineate ocean oil slicks with a texture-classifying neural network algorithm (TCNNA). *Canadian Journal of Remote Sensing*, *35*(5), 411–421.

Garvine, R. W. (1995). A dynamical system for classifying buoyant coastal discharges. *Continental Shelf Research*, *15*(13), 1585–1596.

Garvine, R. W., & Monk, J. D. (1974). Frontal structure of a river plume. *Journal of Geophysical Research*, *79*(15), 2251–2259.

Hamilton, P., Donohue, K. A., Leben, R. R., Lugo-Fernández, A., & Green, R. E. (2011). Loop Current observations during spring and summer of 2010: Description and historical perspective. In *Monitoring and modeling the Deepwater Horizon oil spill: A record-breaking enterprise, Geophysical monograph series* (Vol. 195, pp. 117–130).

Horstmann, J., Nieto Borge, J. C., Seemann, J., Carrasco, R., & Lund, B. (2015). Chapter 16—Wind, wave and current retrieval utilizing X-band marine radars. In Y. Liu, H. Kerkering, & R. H. Weisberg (Eds.), *Coastal ocean observing systems* (pp. 281–304). Boston, MA: Academic.

Hu, C., Lee, Z., & Franz, B. (2012). Chlorophyll *a* algorithms for oligotrophic oceans: A novel approach based on three-band reflectance difference. *Journal of Geophysical Research*, *117*, C01011. https://doi.org/10.1029/2011JC007395

Hu, C., Li, X., Pichel, W. G., & Muller-Karger, F. E. (2009). Detection of natural oil slicks in the NW Gulf of Mexico using MODIS imagery. *Geophysical Research Letters*, *36*, L01604. https://doi.org/10.1029/2008GL036119

Hu, C., Nelson, J. R., Johns, E., Chen, Z., Weisberg, R. H., Müller, et al. (2005). Mississippi River water in the Florida Straits and in the Gulf Stream off Georgia in summer 2004. *Geophysical Research Letters*, *32*, L14606. https://doi.org/10.1029/2005GL022942

Kourafalou, V. H., & Androulidakis, Y. S. (2013). Influence of Mississippi River induced circulation on the Deepwater Horizon oil spill transport. *Journal of Geophysical Research: Oceans*, *118*, 3823–3842. https://doi.org/10.1002/jgrc.20272

Kourafalou, V. H., Oey, L.-Y., Wang, J. D., & Lee, T. N. (1996). The fate of river discharge on the continental shelf. Part I: Modeling the river plume and the inner-shelf coastal current. *Journal of Geophysical Research*, *101*(C2), 3415–3434. https://doi.org/10.1029/95JC03024

Le Hénaff, M., & Kourafalou, V. H. (2016). Mississippi waters reaching South Florida reefs under no flood conditions: Synthesis of observing and modeling system findings. *Ocean Dynamics*, *66*(3), 435–459.

Le Hénaff, M., Kourafalou, V. H., Morel, Y., & Srinivasan, A. (2012b). Simulating the dynamics and intensification of cyclonic Loop Current Frontal Eddies in the Gulf of Mexico. *Journal of Geophysical Research*, *117*, C02034. https://doi.org/10.1029/2011JC007279

Le Hénaff, M., Kourafalou, V. H., Paris, C. B., Helgers, J., Hogan, P. J., & Srinivasan, A. (2012a). Surface evolution of the Deepwater Horizon oil spill: Combined effects of circulation and wind induced drift. *Environmental Science Technology*, *46*, 7267–7273. https://doi.org/10.1021/es301570w

Liu, Y. Y., Weisberg, R. H., Hu, C. C., & Zheng, L. L. (2011). Trajectory forecast as a rapid response to the Deepwater Horizon oil spill. In *Monitoring and modeling the Deepwater Horizon oil spill: A record-breaking enterprise* (pp. 153–165).

Lumpkin, R., Özgökmen, T., & Centurioni, L. (2017). Advances in the application of surface drifters. *Annual Review of Marine Science*, *9*, 59–81.

Lund, B., Graber, H. C., Hessner, K., & Williams, N. J. (2015). On shipboard marine X-band radar near-surface current "calibration." *Journal of Atmospheric and Oceanic Technology*, *32*(10), 1928–1944.

Lund, B., Haus, B. K., Horstmann, J., Graber, H. C., Carrasco, R., Laxague, N. J. M., et al. (2018). Near-surface current mapping by shipboard marine X-band radar: A validation. *Journal of Atmospheric and Oceanic Technology*. https://doi.org/10.1175/JTECH-D-17-0154.1

Mariano, A. J., Ryan, E. H., Huntley, H. S., Laurindo, L. C., Coelho, E., Griffa, A., et al. (2016). Statistical properties of the surface velocity field in the northern Gulf of Mexico sampled by GLAD drifters. *Journal of Geophysical Research: Oceans*, *121*, 5193–5216. https://doi.org/10.1002/2015JC011569

McNutt, M. K., Camilli, R., Crone, T. J., Guthrie, G. D., Hsieh, P. A., Ryerson, T. B., et al. (2012). Review of flow rate estimates of the Deepwater Horizon oil spill. *Proceedings of the National Academy of Sciences of the United States of America*, *109*(50), 20260–20267.

Milliman, J. D., & Meade, R. H. (1983). World-wide delivery of river sediment to the oceans. *The Journal of Geology*, *91*(1), 1–21.

Morey, S. L., Martin, P. J., O'Brien, J. J., Wallcraft, A. A., & Zavala-Hidalgo, J. (2003). Export pathways for river discharged fresh water in the northern Gulf of Mexico. *Journal of Geophysical Research*, *108*(C10), 3303. https://doi.org/10.1029/2002JC001674

Novelli, G., Guigand, C. M., Cousin, C., Ryan, E. H., Laxague, N. J., Dai, H., et al. (2017). A biodegradable surface drifter for ocean sampling on a massive scale. *Journal of Atmospheric and Oceanic Technology*, *34*(11), 2509–2532.

Olascoaga, M. J., Beron-Vera, F. J., Haller, G., Trinanes, J., Iskandarani, M., Coelho, E. F., et al. (2013). Drifter motion in the Gulf of Mexico constrained by altimetric Lagrangian coherent structures. *Geophysical Research Letters*, *40*, 6171–6175. https://doi.org/10.1002/2013GL058624

Ortner, P. B., Lee, T. N., Milne, P. J., Zika, R. G., Clarke, M. E., Podestá, G. P., et al. (1995). Mississippi River flood waters that reached the Gulf Stream. *Journal Geophysical Research*, *100*(C7), 13595–13601. https://doi.org/10.1029/95JC01039

Poje, A. C., Özgökmen, T. M., Lipphardt, B. L., Haus, B. K., Ryan, E. H., Haza, A. C., et al. (2014). Submesoscale dispersion in the vicinity of the Deepwater Horizon spill. *Proceedings of the National Academy of Sciences of the United States of America*, *111*(35), 12693–12698.

Price, J. M., Reed, M., Howard, M. K., Johnson, W. R., Ji, Z. G., Marshall, C. F., et al. (2006). Preliminary assessment of an oil-spill trajectory model using satellite-tracked, oil-spill-simulating drifters. *Environmental Modelling & Software*, *21*(2), 258–270.

Röhrs, J., & Christensen, K. H. (2015). Drift in the uppermost part of the ocean. *Geophysical Research Letters*, *42*, 10349–10356. https://doi.org/10.1002/2015GL066733

Röhrs, J., Christensen, K. H., Hole, L. R., Broström, G., Drivdal, M., & Sundby, S. (2012). Observation-based evaluation of surface wave effects on currents and trajectory forecasts. *Ocean Dynamics*, *62*(10–12), 1519–1533.

Schiller, R. V., & Kourafalou, V. H. (2014). Loop Current impact on the transport of Mississippi River waters. *Journal Coastal Research*, *30*(6), 1287–1306. https://doi.org/10.2112/JCOASTRES-D-13-00025.1

Schiller, R. V., Kourafalou, V. H., Hogan, P., & Walker, N. D. (2011). The dynamics of the Mississippi River plume: Impact of topography, wind and offshore forcing on the fate of plume waters. *Journal of Geophysical Research*, *116*, C06029. https://doi.org/10.1029/2010JC006883

Senet, C. M., Seemann, J., & Ziemer, F. (2001). The near-surface current velocity determined from image sequences of the sea surface. *IEEE Transactions on Geoscience and Remote Sensing*, *39*(3), 492–505.

Smith, R. H., Johns, E. M., Goni, G. J., Trinanes, J., Lumpkin, R., Wood, A. M., et al. (2014). Oceanographic conditions in the Gulf of Mexico in July 2010, during the Deepwater Horizon oil spill. *Continental Shelf Research*, *77*, 118–131.

Socolofsky, S. A., Adams, E. E., & Sherwood, C. R. (2011). Formation dynamics of subsurface hydrocarbon intrusions following the Deepwater Horizon blowout. *Geophysical Research Letters*, *38*, L09602. https://doi.org/10.1029/2011GL047174

Stewart, S. R. (2005). *Tropical cyclone report—Hurricane Ivan 2–24 September 2004*. National Hurricane Center.

Walker, N. D. (1996). Satellite assessment of Mississippi River plume variability: Causes and predictability. *Remote Sensing of Environment*, *58*(1), 21–35.

Walker, N. D., Fargion, G., Rouse, L. J., Jr., & Biggs, D. (1994). Circulation of Mississippi River water discharged into the northern Gulf of Mexico by the great flood of summer 1993. *Eos, Transactions, American Geophysical Union*, *75*(36), 409.

Walker, N. D., Huh, O. K., Rouse, L. J., & Murray, S. P. (1996). Evolution and structure of a coastal squirt off the Mississippi River delta: Northern Gulf of Mexico. *Journal of Geophysical Research*, *101*(C9), 20643–20655.

Walker, N. D., Pilley, C. T., Raghunathan, V. V., D'Sa, E. J., Leben, R. R., Hoffmann, N. G., et al. (2011). Impacts of Loop Current frontal cyclonic eddies and wind forcing on the 2010 Gulf of Mexico oil spill. In *Monitoring and modeling the Deepwater Horizon oil spill: A record-breaking enterprise* (pp. 103–116).

Walker, N. D., Wiseman, W. J., Jr., Rouse, L. J., Jr., & Babin, A. (2005). Effects of river discharge, wind stress, and slope eddies on circulation and the satellite-observed structure of the Mississippi River plume. *Journal of Coastal Research*, *21*, 1228–1244.

Warren, C. J., MacFadyen, A., & Henry Jr, C. (2014). Mapping oil for the destroyed Taylor Energy Site in the Gulf of Mexico. In *International oil spill conference proceedings* (Vol. 2014, No. 1, p. 299931). Washington, DC: American Petroleum Institute.

Wiseman, W. J., Bane, J. M., Murray, S. P., & Tubman, M. W. (1975). Small scale temperature and salinity structure over the inner shelf west of the Mississippi Rive-delta. *Details - Mémoires de la Société royale des sciences de Liège*, *6*, 10.

Young, I. R., Rosenthal, W., & Ziemer, F. (1985). A three-dimensional analysis of marine radar images for the determination of ocean wave directionality and surface currents. *Journal of Geophysical Research*, *90*(C1), 1049–1059.

Zavala-Hidalgo, J., Morey, S. L., O'Brien, J. J., & Zamudio, L. (2006). On the Loop Current eddy shedding variability. *Atmósfera*, *19*(1), 41–48.

Erratum

The originally published version of this article omitted two hyperlinks to data in the Acknowledgments section. This article has been updated, and this may be considered the authoritative version of record.